Lithos 116 (2010) 111–128

Contents lists available at ScienceDirect

Lithos

journal homepage: www.elsevier.com/locate/lithos

Compositionally stratified lithosphere and carbonatite metasomatism recorded in mantle xenoliths from the Western Qinling (Central China)

Ben-Xun Su [a,b,c,*], Hong-Fu Zhang [a], Patrick Asamoah Sakyi [d], Ji-Feng Ying [a], Yan-Jie Tang [a], Yue-Heng Yang [a], Ke-Zhang Qin [b], Yan Xiao [a], Xin-Miao Zhao [a]

[a] State Key Laboratory of Lithospheric Evolution, Institute of Geology and Geophysics, Chinese Academy of Sciences, P.O. Box 9825, Beijing 100029, China
[b] Key Laboratory of Mineral Resources, Institute of Geology and Geophysics, Chinese Academy of Sciences, P.O. Box 9825, Beijing 100029, China
[c] Graduate University of Chinese Academy of Sciences, Beijing 100049, China
[d] Department of Geology, University of Ghana, P.O. Box LG 58, Legon-Accra, Ghana

ARTICLE INFO

Article history:
Received 4 May 2009
Accepted 8 January 2010
Available online 15 January 2010

Keywords:
Carbonatite metasomatism
Mantle peridotite
Stratified lithospheric mantle
Western Qinling

ABSTRACT

In Central China, long-distance effects from collision between the North China and Yangtze cratons, uplift of the Tibetan Plateau and subduction of the Pacific Ocean are believed to converge in the Western Qinling. Mantle xenoliths from Baiguan and Haoti kamafugites in the Western Qinling were investigated to understand the lithospheric structure and mantle metasomatism beneath the orogenic belt. The Western Qinling lithosphere with depths of at least 120 km is geothermally hot and compositionally stratified, companied by a step-wise decrease in fertility with depth. The shallower portion of the lithospheric mantle is represented by type 2 xenoliths which lack alteration and deformation, and have fertile characteristics in compositions. The dominant rock type in the mantle section is the type 1 peridotites, which have had undergone relatively higher melt extraction and subsequent metasomatism.

In-situ trace element data for minerals in the Baiguan and Haoti xenoliths are presented in this study. Baiguan clinopyroxenes have high LREE and show Ba, Th, U, Pb, Sr enrichment and negative Hf and Y anomalies, but the Haoti clinopyroxenes have large variations in trace elements and complicated distributions in LILE, and show negative Ti, Zr and Hf anomalies. Clinopyroxenes from both xenolith types have Ti/Eu and $(La/Yb)_N$ ratios in large ranges of 902–15,813 and 0–20, respectively. The petrological and geochemical characteristics suggest that the Western Qinling peridotites had been subjected to silicate and subsequent carbonatite metasomatism, and that carbonatite metasomatism was predominant in Baiguan but lesser in Haoti. Comparisons with the Western Qinling carbonatites and world-wide carbonatites indicate that carbonatite melts involved in the metasomatism originated from deep mantle and most likely related to carbonatite magma, with contributions from subducted oceanic crust. The type 2 peridotites, comprising clinopyroxene megacrysts and clinopyroxenite display similar trace element abundances and patterns, suggesting a close affinity in petrogenesis.

1. Introduction

Geochemical information about the continental lithospheric mantle is obtained mainly from basalts and/or kimberlites and their entrained xenoliths (e.g., Pearson et al., 2003; Zhang et al., 2008; Francis and Patterson, 2009). These xenolith-hosting volcanic rocks commonly occur within or at the margins of cratons/blocks (e.g., Pearson et al., 2003), and may allow lithospheric structure and evolution to be determined. However, knowledge of the orogenic lithosphere is still ambiguous because of its complex modification and the lack of deep-seated xenoliths.

Many mantle-derived xenoliths have been subjected to mantle metasomatism before entrainment. (e.g., Menzies and Hawkeworth, 1987; Pearson et al., 2003; Zhang, 2005; Ionov et al., 2006; Zhang et al., 2007a,b; Tang et al., 2008). The metasomatism is generally attributed to infiltration and percolation of either silicate melts or H_2O–CO_2-rich fluids, referred to silicate and carbonatite metasomatism, respectively (O'Reilly and Griffin, 1988; Thibault and Edgar, 1990; Franz and Wirth, 1997; Ionov, 2001; Dalou et al., 2009). The effects of silicate metasomatism have been studied in many xenoliths suites based on trace element systematics, and many established indicators are used to evaluate its extent (e.g., Menzies and Hawkeworth, 1987; Thibault and Edgar, 1990; Rudnick et al., 1993; Coltorti et al., 1999; Gorring and Kay, 2000; Downes, 2001; Downes et al., 2004). Carbonatite metasomatism is poorly understood because of the rarity of carbonate owing to its consumption by decarbonation reactions (Green and Wallace, 1988; Dalton and Wood, 1993) and decomposition during xenoliths

* Corresponding author. P.O. Box 9825, Beijing 100029, China. Tel.: +86 10 82998190; fax: +86 10 62010846.
E-mail address: subenxun@mail.igcas.ac.cn (B.-X. Su).

0024-4937/$ – see front matter.
doi:10.1016/j.lithos.2010.01.004

exhumation (Canil, 1991; Rosatellia et al., 2007). Nevertheless, the mass of carbon stored in the mantle exceeds that in all other reservoirs of the global carbon cycle combined (Hammouda, 2003; Dasgupta and Hirschmann, 2006), and for which reason carbonatite metasomatism is probably common within the upper mantle.

Carbonate and some geochemical features interpreted to be associated with carbonatite metasomatism have been observed in a few mantle xenolith suites from some localities (Rudnick et al., 1993; Laurora et al., 2001; Ionov and Harmer, 2002; Rosatellia et al., 2007). However, the differences between the effects of silicate and carbonatite metasomatism are not well established (e.g., Yaxley et al., 1998; Downes, 2001), basically because both agents rarely occur in individual suites and the latter could be overprinted by the former. Actually, such a distinction between silicate and carbonatite metasomatism is important, considering the significant role of the H_2O–CO_2 system in the modification of upper mantle and the genesis of silica-undersaturated basalts (Wyllie, 1989; Dautria et al., 1992; Gasparik and Litvin, 2002; Dasgupta and Hirschmann, 2006; Walter et al., 2008).

We have undertaken a study of mantle xenoliths from two localities, Baiguan and Haoti in the Western Qinling, central China, in order to probe the lithospheric structure beneath an orogenic region and to constrain melt/fluid-peridotite interaction using the trace element composition of the constituent minerals. The lithospheric mantle beneath the Western Qinling probably was modified by both agents successively or simultaneously, which provide us an opportunity to investigate the process and distinguish between silicate and carbonatite metasomatism using trace element of minerals in mantle xenoliths. We report here, the first trace element data of constituent minerals in the Western Qinling xenoliths besides major element data of Baiguan xenoliths.

2. Geology

The Kunlun–Qilian–Qinling–Dabie Mountains, which is the central orogenic belt, is the most important orogenic belt in China. The western part of the central orogen is believed to be the tectonic suture between the Tibetan Plateau and the Tarim and Qaidam blocks (Zhang et al., 2001, 2002a,b), while the eastern part is generated from the North China–South China collision (Gao et al., 1996; Zhou et al., 2000, Xu et al., 2002a,b). The Western Qinling is located in the center of the central orogenic belts and it is an axis for Chinese continents including the North China Craton in the northeast, the Yangtze Craton in the southeast, and the Tibetan Plateau in the southwest (Fig. 1). The Western Qinling is therefore a significant cratonic intersection by displaying signatures of the North China–Yangtze collision and Tibetan uplift (Gao et al., 1996; Zhang et al., 2001; Xu et al., 2002a, b). Recent study of peridotites from Haoti showed garnet–spinel transition zone at 78 km beneath the Western Qinling to be significantly thicker than the 55–72 km zone beneath eastern China (Su et al., 2007), suggesting that either lithospheric thinning did not take place or took place on a small-scale beneath the Western Qinling. However, the lithospheric structure beneath the Western Qinling has not yet been established and its characteristics are still unknown.

The Baiguan and Haoti cinder cones are part of the Cenozoic volcanism associated with the Tianshui–Lixian fault in the Western Qinling (Zhang et al., 2001; Yu et al., 2003, 2004, 2005; Dong et al., 2008). These volcanoes are comprised of kamafugite lavas and associated carbonatites dated at 7.1–23 Ma (Yu et al., 2001, 2005). These ages are comparable with xenolith-hosting volcanic rocks within the Tibetan Plateau and its adjacent regions, including Jianchuan–Dali, Pulu, and Maguan (Wang et al., 2002; Zhang et al., 2002a,b; Xia and Xu, 2006), and suggest a possible relationship with uplift of the Tibetan Plateau. Xenoliths, including garnet lherzolite, spinel lherzolite, wehrlite, dunite, websterite and clinopyroxenite, entrained in Haoti kamafugites revealed the existence of two types (type 1 and type 2) of suites (Su et al., 2009). Separate suites of Haoti xenoliths and xenocrysts previously been described by Yu et al. (2001), Shi et al. (2003) and Su et al. (2006a, 2007, 2009), form the basis of the current study. In this paper, we will focus on the Baiguan xenoliths and comparison with the Haoti samples to reconstruct the structure of the lithosphere and to further constrain the agents of metasomatism.

3. Petrology

The Western Qinling xenoliths can be subdivided into type 1 and 2, based on forsterite (Fo) content of their olivine (type 1, Fo > 90; type 2, Fo ≤ 90). This definition differs from the classification by Lloyd (1987).

3.1. Type 1

The type 1 xenoliths from Baiguan are spinel lherzolite, subordinate garnet ± spinel lherzolite and dunite (Table 1), while the Haoti xenoliths consist of spinel-bearing/free lherzolite, garnet lherzolite, wehrlite, websterite, clinopyroxenite and clinopyroxene megacryst (Su et al., 2009). Some of the xenoliths are very small and could simply be fragments of larger xenoliths disaggregated during transport. Compared to xenoliths from Haoti, some of the Baiguan xenoliths are somewhat altered, which could be attributed to very late hydrothermal or weathering activity. In hand-specimen, some samples display grey-white or red color with opaque material such as ilmenite, barite, serpentinite or iddingsite and without apparent crystal shape along major grain boundaries. Most silicate minerals have wide and irregularly altered margins and reaction rims as shown in Fig. 2A–F. Serpentinization commonly occurs and serpentines are shown around or within residual olivines (Fig. 2A, C, F). Olivine is absent in samples BG23B and BG23S, because of strong alteration. Orthopyroxenes are usually rounded (Fig. 2B), although they occasionally display irregular shapes (Fig. 2F). Deformed structures such as kink bands in olivines, mineral elongation and orientation, and mechanical breakdown (Fig. 2A–D) which occur in the Haoti xenoliths (Su et al., 2009) are also observed in Baiguan xenoliths. Clinopyroxenes are broken into many irregular fragments (Fig. 2D) and they rarely preserve their original habit (Fig. 2E). In spite of the strong alteration and deformation, fresh grains are considered to record the original compositions of the minerals. Garnets occur as discrete, round grains and are composed of corona assemblage of very fine clinopyroxene, orthopyroxene and spinel, and residual core (Fig. 2E). The residual garnets occur in samples BG6 and BG8, and the imprint of previously existing garnet is recorded in the fine-grained spinel and pyroxene assemblage in several spinel lherzolites.

3.2. Type 2

One type 2 xenolith sample (BG5-2) in this study, collected from Baiguan is fresh and exhibits fine-grained equigranular texture and other features very similar to those in type 2 xenoliths from Haoti (Su et al., 2009). Triple junction and identifiable boundaries between major minerals are also observed (Fig. 2G). Some olivines display undulose extinction due to kink-banding (Fig. 2H).

3.3. Textural features in Baiguan and Haoti xenoliths

There are metasomatic features to interpret the textures in Baiguan and Haoti xenoliths. Calcite is a universal accessory mineral, occurring both as veins and discrete grains. Vein calcite occurs in fractures in olivine and clinopyroxene (Fig. 3A) and generally extends into composite melt pockets. The melt pockets are composed of fine-grained olivine and clinopyroxene, and occasionally discrete-grained calcite, barite, apatite or alkaline glass (Fig. 3B). In a few cases, discrete calcite grains associated with barite occur in contact with

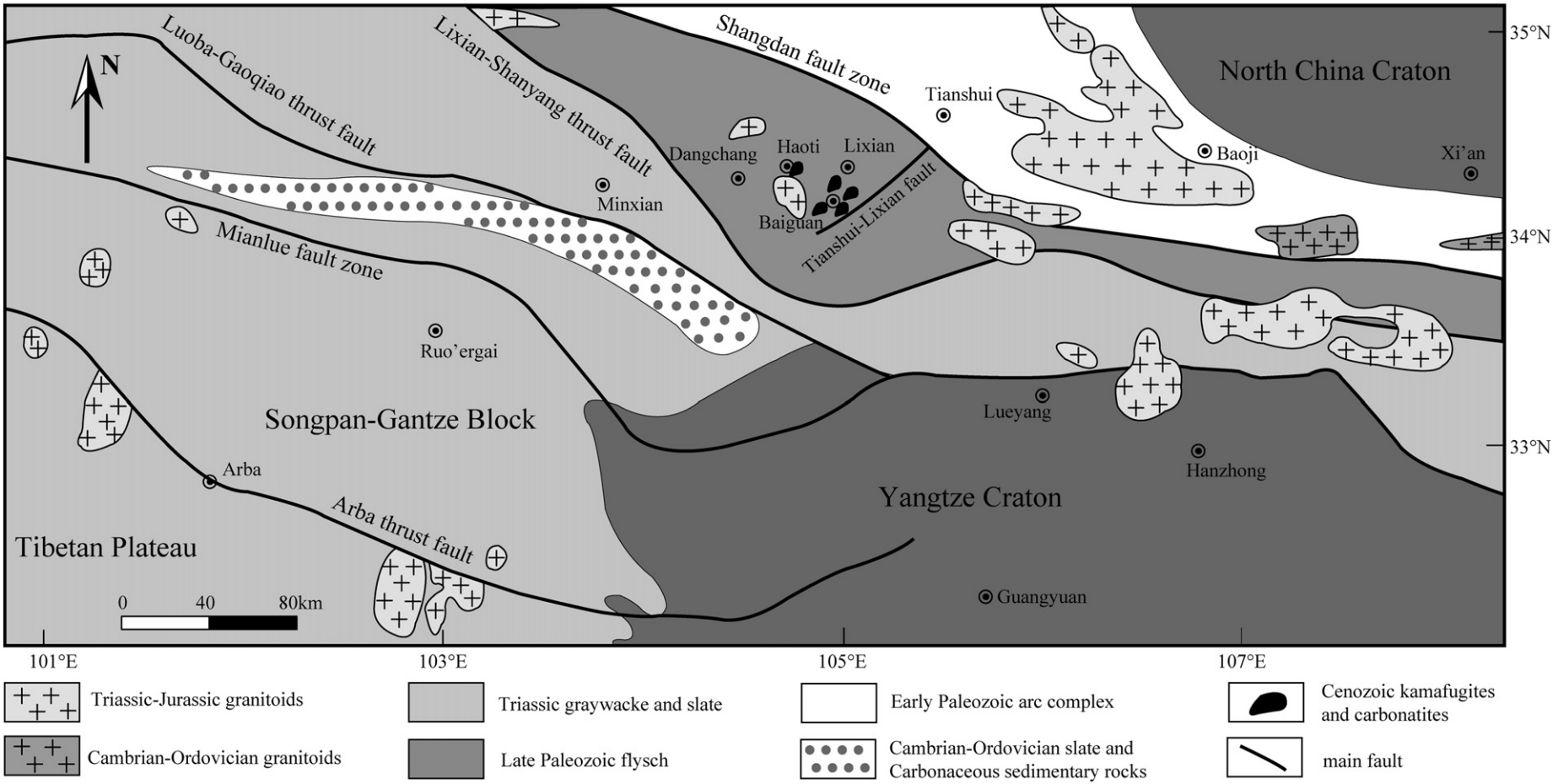

Fig. 1. Geologic sketch map of the Western Qinling and its adjacent regions (modified from Zhang et al., 2001; Mao et al., 2002).

Table 1
Petrologic features of mantle xenoliths from Baiguan, Lixian, Western Qinling.

Sample	Rock type	Alteration	Size (cm × cm)	Mineral assemblage
Type 1				
BG1	Sp lherzolite	Fresh	1.0 × 0.5	Ol, Opx, Cpx, Sp, Ilme, Apat and Ca
BG4	Lherzolite	Fresh	1.3 × 1.2	Ol, Opx and Cpx
BG5-1	Lherzolite	Fresh	1.0 × 0.5	Ol, Opx, Cpx and Ca
BG6	Grt lherzolite	Fresh	1.4 × 0.5	Ol, Opx, Cpx, Grt, Sp and Ca
BG8	Grt lherzolite	Weakly-serpentinized	2.0 × 1.4	Ol, Opx, Cpx, Grt and Sp
BG9	Sp lherzolite	Weakly-serpentinized	2.5 × 1.5	Ol, Opx, Cpx, Sp and Ca
BG11	Sp lherzolite	Serpentinized	2.2 × 1.5	Ol, Opx, Cpx and Sp
BG21B	Lherzolite	Fresh	2.5 × 1.5	Ol, Opx, Cpx, Ba and Ca
BG21S	Lherzolite	Weakly-serpentinized	1.2 × 0.7	Ol, Opx, Cpx, Sp, Ba and Ca
BG23B	Sp lherzolite	Serpentinized	1.5 × 1.3	Ol (gone), Opx, Cpx, Sp and Ca
BG23S	Sp lherzolite	Serpentinized	1.0 × 0.5	Ol (gone), Opx, Cpx, Sp and Ca
BG24	Lherzolite	Serpentinized	1.2 × 1.0	Ol, Opx, Cpx, Sp and Ca
BG40	Dunite	Fresh	0.5 × 0.5	Ol
Type 2				
BG5-2	Sp lherzolite	Fresh	2.8 × 2.0	Ol, Opx, Cpx, Sp and Ca

Note: Ilme, ilmenite; Apat, apatite; Ca, carbonate; and Sp, spinel.

orthopyroxene (Fig. 3C, sample BG21B). In this sample BG21B, round ilmenite grains are observed as well (Fig. 3D). In comparison, the "metasomatic" assemblage in Haoti xenoliths is different and more complex. Accessory minerals in Haoti xenoliths are Fe-rich chromite, pyrite and ilmenite, and hydrous amphibole and phlogopite without calcite. These trace minerals in melt pocket are inferred to be secondary. One phlogopite set in silicate minerals in wehrlite sample HT-44 is not coexisting with metasomatic minerals and has lower trace element abundances, suggesting that it probably formed in an earlier stage relative to other phlogopites. The notable point is that the sample HT-16 described in Su et al. (2009) contains amphibole, phlogopite and chromite, combined with other minerals such as high-Na clinopyroxene and high Ti spinel, demonstrating the strongest metasomatism. The Haoti xenoliths contain abundant composite pockets of melts, which are generally composed of recrystallized olivine, clinopyroxene, alkaline glass, accessory minerals mentioned above and rare residual olivine or orthopyroxene (Fig. 3E, F). The recrystallized olivine and clinopyroxene are characterized by high Ca and Mg# number. These petrological and geochemical features demonstrate that metasomatism modified the lithospheric mantle beneath the Western Qinling.

4. Mineral chemistry

4.1. Major element of minerals in Baiguan xenoliths

4.1.1. Olivine

Compositions of selected fresh and unaltered grains are generally homogeneous within a given sample. Olivines in Baiguan type 1 xenoliths have Fo (Fo = Mg/(Mg + Fe) × 100) contents in a range of 90.4–92.2, and CaO and NiO in range of 0.04–0.12 wt.% and 0.27–0.62 wt.%, respectively (Fig. 4A; Table 2). These variations are relatively larger than those in Haoti xenoliths. The Baiguan type 2 olivine has Fo, CaO and NiO contents of 89.5, 0.06 wt.% and 0.40 wt.% respectively, and are comparable to those in Haoti type 2 xenoliths.

4.1.2. Clinopyroxene

The primary clinopyroxenes in the type 1 xenoliths differ in composition from secondary ones, especially in TiO_2, Al_2O_3 and CaO contents (Table 2). Secondary clinopyroxenes have higher TiO_2 and Al_2O_3 contents and lower CaO than primary grains. Mg# numbers of the primary clinopyroxene vary between 91.7 and 93.9 and have no correlation with Cr# numbers. Na_2O in both types of clinopyroxenes ranges from 0.2 wt.% to 1.8 wt.% and shows a positive correlation with Al_2O_3 (Fig. 4B). The type 1 clinopyroxenes are somewhat refractory and display metasomatic trend compared to the type 2 ones (Fig. 4B).

In a few samples, clinopyroxenes exhibit compositional zoning as shown by profiles on two grains, namely BG21B and BG21S. The compositional profile of BG21B clinopyroxene demonstrates that TiO_2 and Na_2O increase from core to rim whereas Mg# and Cr_2O_3 decrease (Fig. 5A; Appendix A). The rim of BG21S grain is depleted in TiO_2 and Na_2O and enriched in Mg# and Cr_2O_3 relative to the core (Fig. 5B; Appendix A).

4.1.3. Orthopyroxene

Baiguan orthopyroxenes have relative higher CaO contents for a given Al_2O_3 content than the Haoti orthopyroxenes. In most samples, orthopyroxenes have higher CaO and Al_2O_3 than world-wide spinel peridotite and garnet peridotite (Boyd, 1989), and thus plot outside of both fields (Fig. 4C).

Orthopyroxenes in type 2 xenoliths have lower CaO contents and estimated temperatures than those in type 1 (Tables 2 and 4; Su et al., 2009). Both orthopyroxene grains are enriched in CaO on the rims regardless of the clinopyroxene composition in the given sample (Fig. 5C, D).

4.1.4. Garnet

Garnets from two Baiguan samples and an additional one from Haoti are pyropic, with CaO between 3.11 and 5.19 wt.% and Cr_2O_3 from 2.35 to 4.71 wt.% (Table 2; Su et al., 2009). The formation of the outer coronal assemblage undoubtedly involved heating and chemical exchange. Temperature estimation suggests that the coronal assemblages formed at temperatures higher than 1350 °C (Su et al., 2007). The garnet in BG8 is obviously kelyphitised as indicated by the high Na_2O content. We, thus infer that transient heating aided in the decomposition of garnet to form the outer corona.

4.1.5. Spinel

Spinels are apparently distinctive in types 1 and 2 xenoliths (Fig. 4D). The type 1 spinels are fine-grained (less than 100 μm) and show large Cr# variation from 36 to 68, lying in between those from typical spinel peridotites in alkali basalts (Cr# lower than 60) and those from garnet peridotite (Cr# between 60–90) (Boyd, 1989). The type 2 spinels occur in relatively large-sizes and have Cr# of lower than 20.

4.2. Trace element of minerals in Haoti and Baiguan xenoliths

In-situ trace element analyses of clinopyroxene, phlogopite and amphibole are presented in Table 3 and illustrated in Figs. 6 and 7. Calcite could not be analyzed because of its tiny grain, generally less than 40 μm in size of laser beam spot.

Fig. 2. Petrophotographs of the Baiguan xenoliths. Type 1: A) BG4, serpentinized feature and kink band in olivine; B) BG21S, porphyroclastic olivine and orthopyroxene set in fine-grained olivine and pyroxenes; C) BG21B, long-platy olivine with straight boundary; D) BG21B, oriented olivine and clinopyroxene with mechanical comminution feature; E) BG6, relict garnet coexisting with olivine and clinopyroxene; F) interstitial orthopyroxene showing reaction with host rock and slightly curved boundary with olivine; Type 2: G) BG5-2, fine-grained texture and triple junction between major minerals; H) BG5-2, mosaic texture and curved boundary between orthopyroxene and kink-banded olivine.

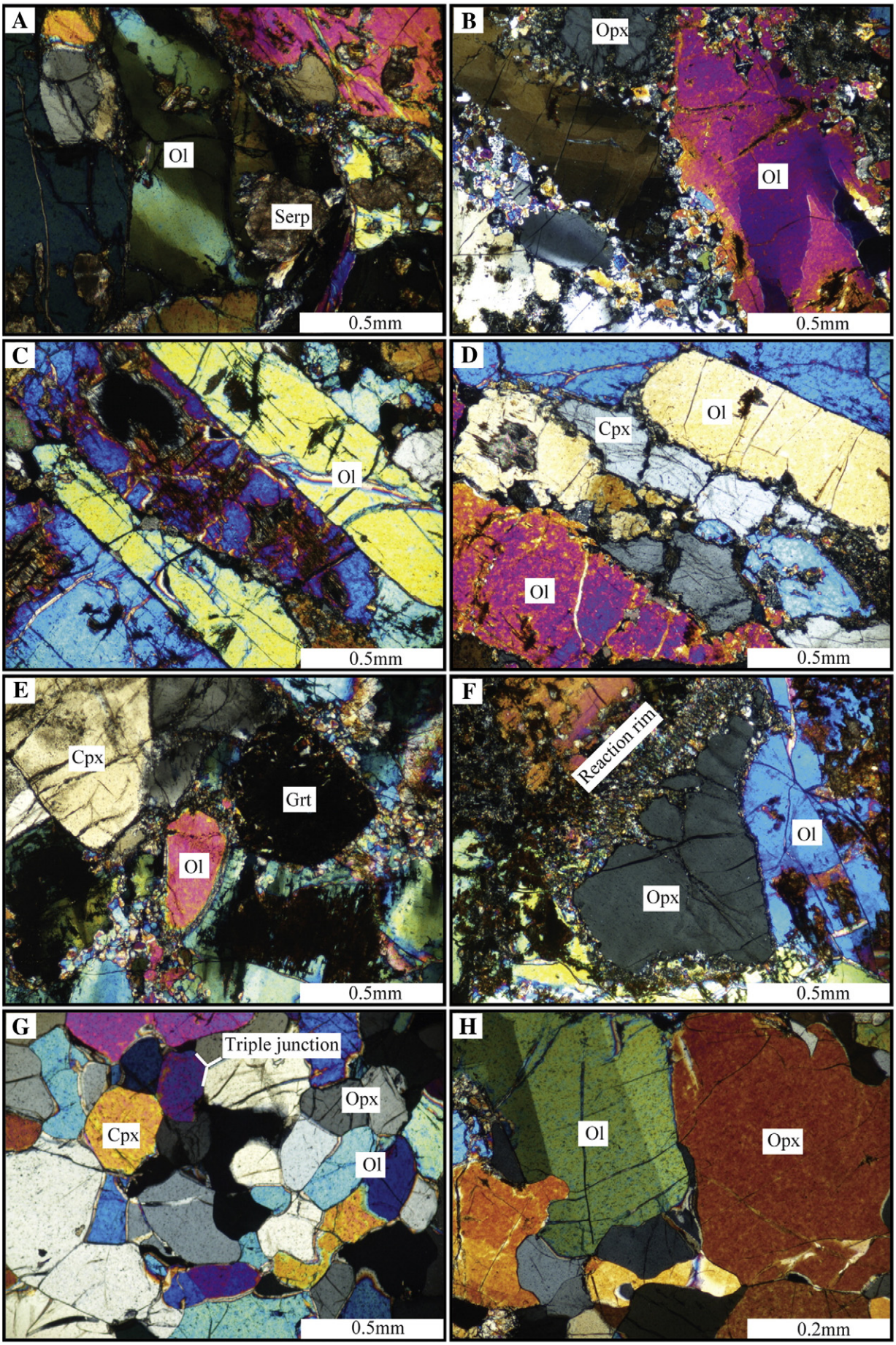
A
Ol
Serp
0.5mm
B
Opx
Ol
0.5mm
C
Ol
0.5mm
D
Cpx
Ol
Ol
0.5mm
E
Cpx
Grt
Ol
0.5mm
F
Reaction rim
Ol
Opx
0.5mm
G
Triple junction
Opx
Cpx
Ol
0.5mm
H
Ol
Opx
0.2mm

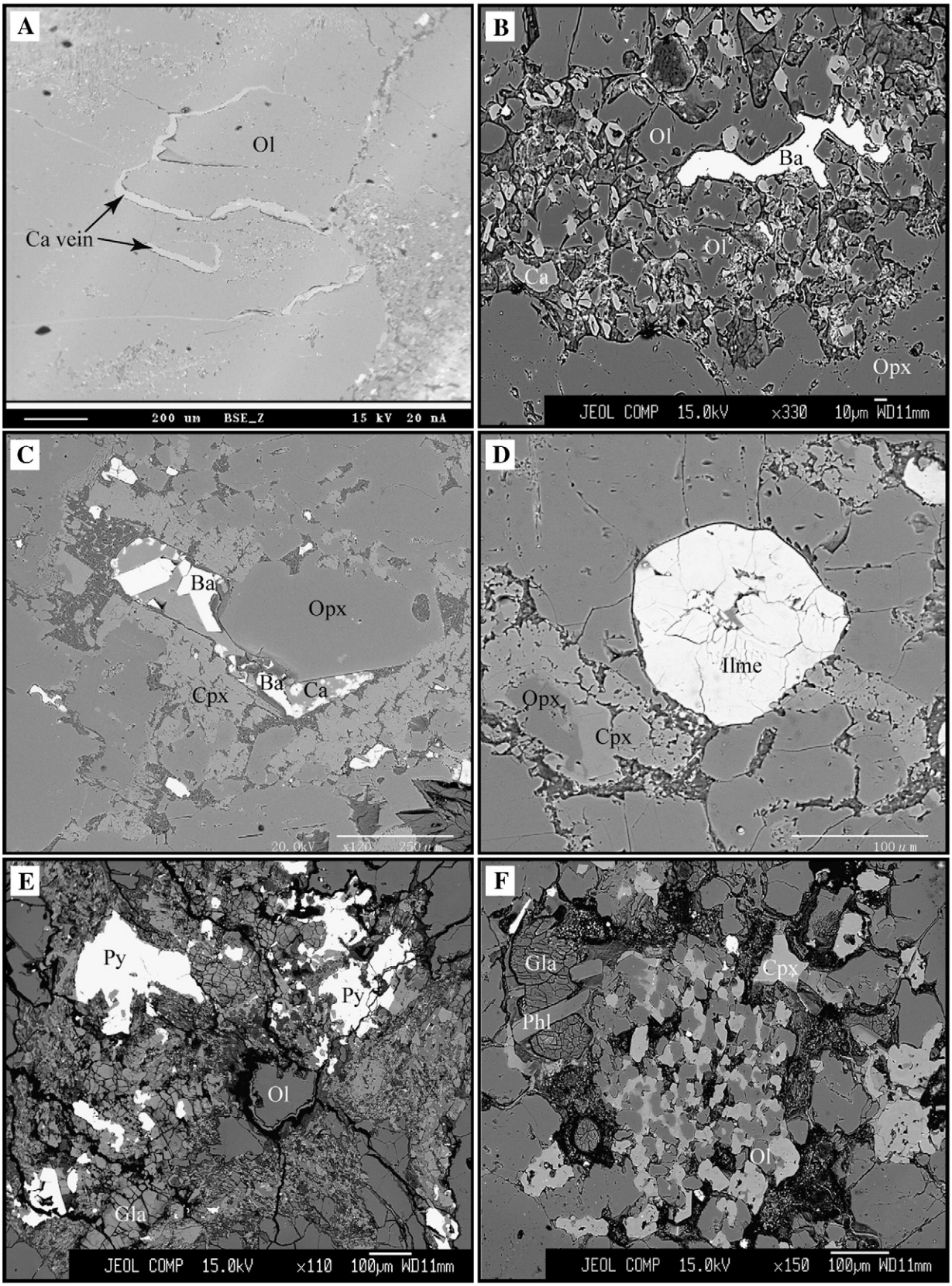

Fig. 3. Petrological feature of carbonatite and silicate metasomatism in mantle xenolith from the Western Qinling (back-scattered image). A) Sample BG6, calcite (Ca) vein in olivine (Ol) and grain boundary; B) Sample BG08-1 (new collection), composite pocket in primary orthopyroxene (Opx) composed of calcite, barite (Ba) and recrystallized and fine-grained olivine; C) and D) Sample BG21B, calcite and barite reacted with orthopyroxene to produce clinopyroxene (C), and round-shaped ilmenite (Ilme) and newly-growing clinopyroxene at the expense of orthopyroxene (D); E) Sample HT08-1 (new collection), pyrite (Py) present in alkaline glass (Gla) surrounding relict olivine; F) Sample HT08-5 (new collection), composite pocket consisting of alkaline glass, phlogopite (Phl), and fine-grained olivine and clinopyroxene.

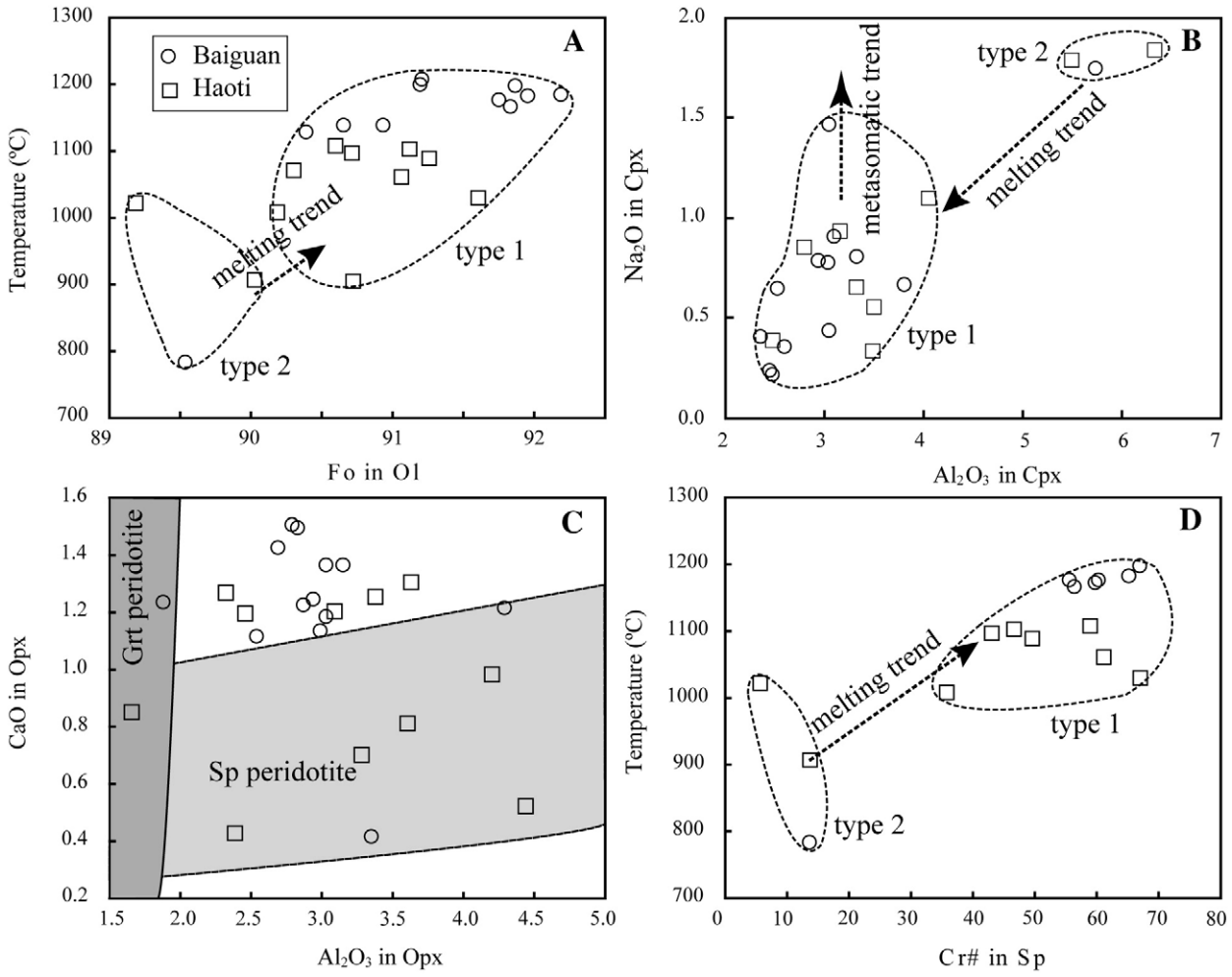

Fig. 4. A) Plot of Fo (forsterite) in olivine of type 1 and type 2 against temperature. B) Plot of Al_2O_3 against Na_2O in clinopyroxenes from Baiguan and Haoti xenoliths. C) Orthopyroxene composition compared to fields of garnet and spinel peridotites (Boyd, 1989). D) Cr# in spinel of type 1 and type 2 plotted against temperature.

4.2.1. Baiguan

Baiguan type 1 clinopyroxenes have LREE-enriched patterns and a wide range of chondrite-normalized abundances (REE_N = 70–230; Fig. 6A, Table 3). Clinopyroxenes in lherzolite (BG21B) and garnet (gone) lherzolite (BG8) display similar fractionated LREE–HREE patterns and lower abundances, whereas BG6 clinopyroxene and rim of BG8 clinopyroxene have relatively higher abundances and lower LREE/HREE fractionation ($(La/Yb)_N$ = 3.2–4.5) (Fig. 6A). The Baiguan type 1 clinopyroxenes are rich in large ion lithophile elements (LILE; Ba, U, Sr, Pb) and depleted in high field strength elements (HFSE; Ta, Zr, Hf) (Fig. 7A). In an individual sample, clinopyroxene rims are more enriched in trace elements, especially in LREE and LILE than the core. In particular, these core–rim compositional variations are eminent in the weakly-serpenitinized sample BG8 (Figs. 6A and 7A).

The type 2 clinopyroxene in spinel lherzolite (BG5-2) has LREE-enriched and convex-upward pattern, and is highly-fractionated between LREE in HREE ($(La/Yb)_N$ > 8; Fig. 6A, Table 3). Similar to the type 1, the type 2 clinopyroxene is rich in Ba, Sr and Y, and depleted in Ta, Zr, Hf and Ti (Fig. 7A). Weak negative Pb anomaly in BG5-2 clinopyroxene occurs in the core but no anomaly is observed in the rim (Fig. 7A), with similar trace element abundances (Figs. 6A and 7A), which are consistent with petrological observation (lack of zoning texture) and major element analyses (almost homogeneous composition). Normalized REE and spider patterns are similar to Cenozoic carbonatites outcropping in the Western Qinling as shown below.

4.2.2. Haoti

The Haoti xenolith suite has complex trace element variations. It can be classified into four groups and plotted as follows: (i) type 2 spinel lherzolite (HT-04 and HT-24; Figs. 6B and 7B), (ii) type 1 spinel-bearing/free lherzolite (HT-08, HT-15, HT-16, HT-23, HT-35 and HT-46; Figs. 6C and 7C), (iii) clinopyroxene-dominated group including wehrlite (HT-44), (iv) clinopyroxenite (HT-14) and clinopyroxene megacryst (HT-7 and HT-31) (Figs. 6D and 7D), and accessory minerals (Figs. 6E and 7E) including phlogopite and amphibole.

HT-04 clinopyroxene has significantly lower LREE, LILE (Rb, Ba, U, Sr) and HFSE (Nb, Ta) abundances in the core but similar HREE, Ti and Y abundances as that of the rim (Figs. 6B and 7B). HT-24 clinopyroxene has higher HREE abundances than HT-04 clinopyroxene and similar patterns in core and rim. The core of HT-24 clinopyroxene shows greatly enriched LREE ($(La/Yb)_N$ = 13), HREE-depleted and convex-shaped pattern, however, its rim has higher trace element abundances and particularly positive Ba anomaly (Figs. 6B and 7B; Table 3).

Clinopyroxenes in spinel-bearing/free lherzolites of type 1 suite have large range of trace element abundances and diverse patterns. REE_N abundances vary from 43 ppm in HT-15 to 1542 ppm in HT-16, and $(La/Yb)_N$ ratios vary from 2.3 to 20 (Table 3). REE patterns are basically LREE-enriched, HREE-flatted and mostly convex-upward (Fig. 6C). The higher REE abundances confirm the more LREE-enriched and LREE–HREE fractionated patterns. LILE (Rb, Ba, U, Th, Pb) and HFSE (Nb, Ta) have discordant abundances and patterns. Although Ba and Pb occur as positive anomaly in HT-16, negative anomalies are

Table 2
Mineral compositions of representative xenoliths from Baiguan, Lixian, Western Qinling.

Sample	BG5-2				BG1				BG4			BG5-1		
rock type	Sp lherzolite				Sp lherzolite				Lherzolite			Lherzolite		
mineral	Ol	Cpx	Opx	Sp	Ol	Cpx	Opx	Sp	Ol	Cpx	Opx	Ol	Cpx	Opx
SiO_2	40.4	52.7	55.5		41.7	53.2	56.2		40.9	53.6	56.3	41.3	53.5	56.2
TiO_2		0.18	0.00	0.05		0.05	0.00	0.17		0.32	0.06			
Al_2O_3		5.75	3.36	55.3		3.06	3.04	24.2		2.37	2.55		2.46	2.70
Cr_2O_3		1.05	0.30	13.3		0.93	0.79	45.5		1.05	0.64		1.17	0.95
FeO	10.0	2.20	6.22	10.5	7.96	2.36	4.95	13.2	7.60	2.57	5.07	8.68	2.84	5.46
MnO	0.28	0.16	0.19	0.17	0.23	0.39	0.15	0.00	0.01	0.25	0.32	0.08	0.07	0.11
MgO	48.3	14.8	33.0	19.4	49.7	19.2	33.3	16.0	50.4	19.5	34.0	48.9	18.9	33.0
CaO	0.06	21.6	0.41		0.05	19.5	1.36		0.05	19.4	1.11	0.12	20.7	1.42
Na_2O		1.74	0.00			0.43	0.16			0.40	0.04		0.23	
NiO	0.61				0.31				0.29			0.42		
Total	99.6	100.2	99.0	98.7	100.0	99.2	100.0	99.1	99.3	99.4	100.0	99.5	99.9	99.8
O=	4	6	6	4	4	6	6	4	4	6	6	4	6	6
Si	0.998	1.905	1.933		1.013	1.932	1.935		1.000	1.942	1.938	1.012	1.937	1.942
Ti		0.005	0.000	0.001		0.001	0.000	0.004		0.009	0.002		0.000	0.000
Al		0.245	0.138	1.721		0.131	0.123	0.865		0.101	0.104		0.105	0.110
Cr		0.030	0.008	0.278		0.027	0.022	1.091		0.030	0.017		0.033	0.026
Fe^{2+}	0.208	0.067	0.181	0.232	0.162	0.072	0.143	0.334	0.155	0.078	0.146	0.178	0.086	0.158
Mn	0.006	0.005	0.006	0.004	0.005	0.012	0.004	0.000	0.000	0.008	0.009	0.002	0.002	0.003
Mg	1.778	0.798	1.713	0.764	1.800	1.039	1.711	0.724	1.836	1.050	1.743	1.786	1.020	1.699
Ca	0.002	0.837	0.015		0.001	0.758	0.050		0.001	0.752	0.041	0.003	0.803	0.053
Na		0.122	0.000			0.030	0.011			0.028	0.003		0.016	0.000
Ni	0.012				0.006				0.006			0.008		
Total	3.002	4.013	3.994	2.999	2.987	4.003	3.998	3.018	3.000	3.998	4.002	2.988	4.002	3.990
Mg#	89.5	92.3	90.4	76.7	91.8	93.6	92.3	68.4	92.2	93.1	92.3	90.9	92.2	91.5
Cr#		10.9	5.7	13.9		16.9	14.8	55.8		22.9	14.4		24.2	19.1

BG6							BG21B			BG21S			
Grt lherzolite							Lherzoltie			Lherzolite			
Ol	Cpx	2nd-Cpx	Opx	2nd-Opx	Grt	2nd-Sp	Ol	Cpx	Opx	Ol	Cpx	Opx	2nd-Sp
40.4	53.5	50.3	56.1	51.0	41.5		40.9	53.4	54.7	41.2	53.9	55.5	
	0.28	0.80	0.00	0.36	0.20	0.11		0.03	0.05		0.06	0.19	0.62
	2.49	8.47	2.95	7.86	18.4	49.9		2.95	4.30		3.82	3.04	52.1
	1.25	1.39	0.69	1.23	4.71	18.4		1.18	0.75		1.09	0.64	13.6
8.53	2.94	3.78	5.21	6.17	6.77	11.1	9.18	2.55	5.37	8.42	2.80	5.17	11.7
0.00	0.25	0.24	0.26	0.58	0.39	0.28	0.09	0.17	0.00	0.19	0.03	0.00	0.00
49.6	19.1	16.9	33.1	29.7	23.8	19.9	48.5	18.5	33.0	49.1	18.9	32.7	21.0
0.12	19.4	17.0	1.24	2.22	3.78		0.11	19.8	1.21	0.12	18.6	1.18	
	0.21	1.17	0.06	0.46	0.22			0.78	0.15		0.66	0.34	
0.32							0.37			0.27			
99.0	99.4	100.0	99.6	99.6	99.7	99.7	99.2	99.4	99.5	99.2	99.8	98.8	99.0
4	6	6	6	6	12	4	4	6	6	4	6	6	4
0.996	1.941	1.815	1.939	1.794	2.980	0.000	1.008	1.938	1.896	1.010	1.936	1.936	
	0.008	0.022	0.000	0.010	0.011	0.002		0.001	0.001		0.002	0.005	0.012
	0.106	0.360	0.120	0.326	1.555	1.576		0.126	0.176		0.162	0.125	1.635
	0.036	0.040	0.019	0.034	0.267	0.389		0.034	0.021		0.031	0.018	0.285
0.176	0.089	0.114	0.151	0.181	0.407	0.249	0.189	0.077	0.156	0.173	0.084	0.151	0.260
0.000	0.008	0.007	0.008	0.017	0.024	0.006	0.002	0.005	0.000	0.004	0.001	0.000	0.000
1.823	1.033	0.907	1.707	1.555	2.548	0.793	1.782	1.003	1.704	1.795	1.012	1.698	0.834
0.003	0.752	0.657	0.046	0.084	0.291		0.003	0.769	0.045	0.003	0.716	0.044	
	0.015	0.082	0.004	0.031	0.031			0.055	0.010		0.046	0.023	
0.006							0.007			0.005			
3.004	3.988	4.004	3.994	4.032	8.113	3.015	2.992	4.008	4.009	2.990	4.008	3.999	3.027
91.2	92.1	88.8	91.9	89.6	86.2	76.1	90.4	92.8	91.6	91.2	92.3	91.8	76.3
	25.2	9.9	13.6	9.5	14.7	19.8		21.2	10.5		16.1	12.4	14.8

Note: Mg# = Mg/(Mg + Fe) × 100;Cr# = Cr/(Cr + Al)×100; analyzed by Cameca SX50 at the Institute of Geology and Geophysics, Chinese Academy of Sciences. More analytical details were described in Su et al., 2009.

common in most clinopyroxenes. Compared to type 2 clinopyroxenes the negative Ti anomaly and Zr, and Hf anomalies in most type 1 clinopyroxenes, are not conspicuous (Fig. 7C).

In clinopyroxene-dominated group, individual samples have the same composition of clinopyroxene, but there is variation between samples. Two clinopyroxene megacryst samples (HT-07 and HT-31) display nearly the same flat pattern ($(La/Yb)_N$ = ~2.5), negative Zr, and Pb and positive Y anomalies, but the absolute abundances or degrees of enrichment/depletion are quite different. Different patterns in Ba and Sr anomalies are also observed (Figs. 6D and 7D).

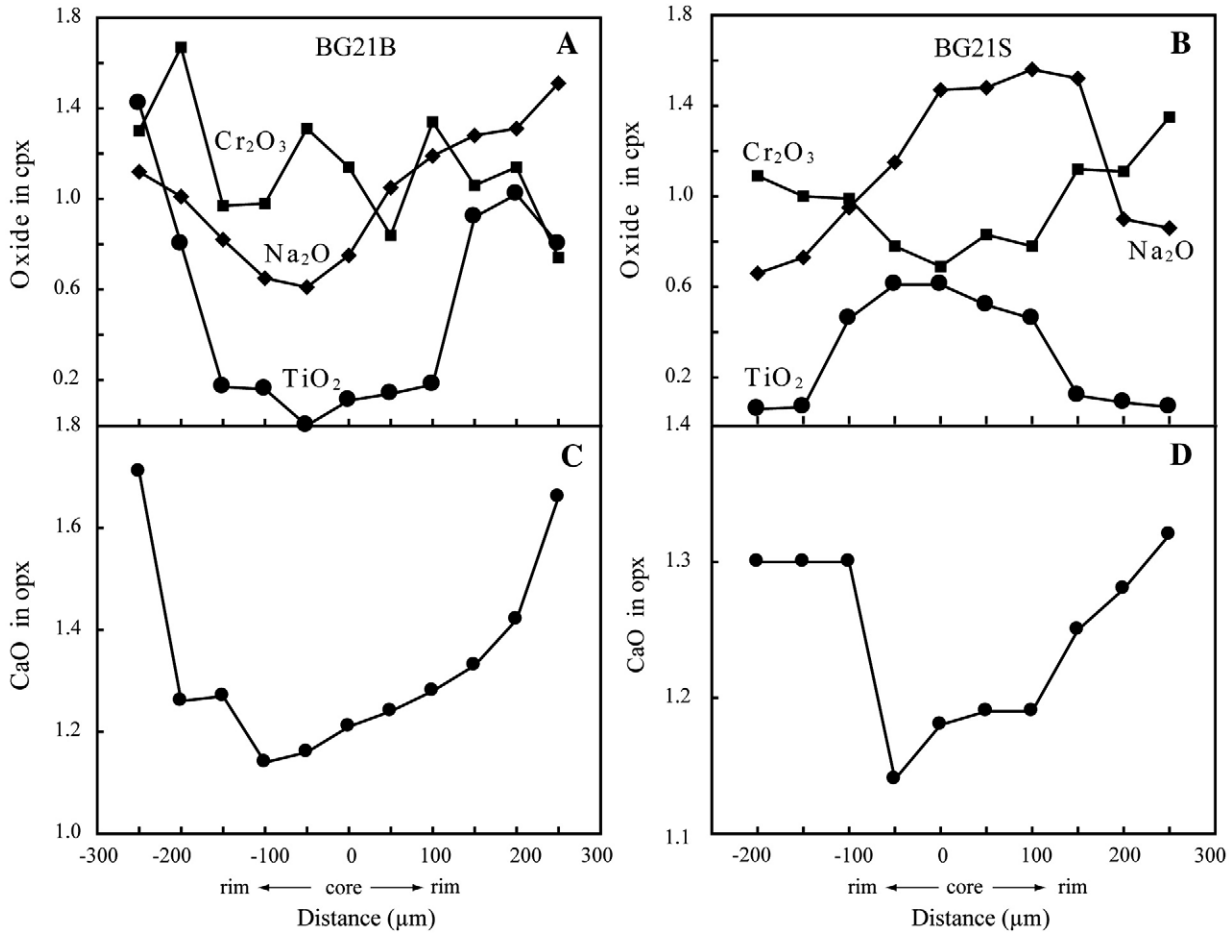

Fig. 5. Compositional variations in rim–core–rim profiles across clinopyroxene and orthopyroxene grains in two peridotitic xenoliths determined by electron-probe analyses.

Clinopyroxenite (HT-14) has moderate trace element abundances and similar patterns to the megacrysts, indicating similarities in their genesis. Clinopyroxene in wehrlite (HT-44) has the lowest REE_N (core, 27; rim, 31) and significantly higher Th, U, Nb, Ta abundances. In contrast to others in this group, REE patterns in HT-44 have concave and slightly Eu-depleted features, and positive Pb, and Sr, and negative Hf, and Ti anomalies appear in spider diagram without Y anomaly. These features in wehrlite are quite similar to those in the type 1 lherzolites.

Phlogopite and amphibole are the main reservoirs for trace elements. Secondary phlogopite in lherzolite sample HT-46 is particularly rich in trace elements and Rb, K and Ti, and has positive Eu anomaly in REE pattern (Fig. 6E), and positive Ba, Nb, Ta, Pb, Sr, Ti anomalies in spider diagram (Fig. 7E). Similar features, except for Eu anomaly are present in phlogopite of HT-23. However, the phlogopite in HT-44 has extremely lower trace element abundances but still shows similar patterns (Figs. 6E and 7E). In contrast, trace element patterns of amphibole mainly exhibit negative anomalies of Eu, Ba, Nb, Ta, Pb, Sr and Ti.

4.2.3. Western Qinling carbonatites

The Western Qinling carbonatite data from Yu et al. (2003) are also presented here for comparison and discussion. Like other world-wide carbonatites (e.g., Dorowa and Shawa, Harmer et al., 1998; Laiwu-Zibo, Ying et al., 2004 and references therein), the REEs show LREE enrichment, and distinctive features of slight negative Eu anomaly (Fig. 6F) and large variation in abundance of the Western Qinling carbonatites. In spider diagram, Ba, U, Pb, Ti, and Y display positive anomalies but Nb, Sr, Nd, Zr anomalies are complicated (Fig. 7F).

5. Discussion

5.1. Thermal state and thickness of lithosphere beneath Western Qinling

The estimated temperatures and pressures of the Western Qinling xenoliths are presented in Table 4 and the detailed calculation procedure is described elsewhere (Su et al., 2009) and Table 4. Pressure estimate was not done on Baiguan spinel-facies peridotites because of their alteration and the fact that some spinels were probably derived from earlier garnet. Pressures of Haoti spinel peridotites were estimated for references using barometer of Ca in olivine (Kohler and Brey, 1990). Spinel-bearing/free peridotites in histogram have a temperature peak (T(W), Wells, 1977) between 1100 and 1200 °C and subordinate temperature in the range of 1000–1200 °C. The type 2 peridotites occupy the lowest part of the temperature field (Fig. 8). Garnet peridotites show a restricted temperature range of 1070–1250 °C and relatively large pressure range of 2.1–3.85 GPa (Table 4; Su et al., 2009), and mostly plot above the typical cratonic and oceanic geotherm but below the Eastern China Cenozoic geotherm (Fig. 8A; Su et al., 2007). The Western Qinling geotherm drawn based on data distribution appears to be parallel to the oceanic geotherm, implying that deeper lithosphere beneath this region is hot and has oceanic lithosphere-like characteristics. In addition, the Western Qinling kamafugites and coexisting carbonatites have ocean island basalt (OIB)-like features in trace

Table 3
Trace element concentrations (ppm) of minerals in the Western Qinling xenoliths.

Sample	BG5-2 SLH		BG6 GLH	BG8 GLH		BG21B LH		HT-04 SLH		HT-07 CPM	HT-24 SLH			HT-08 Sp LH	
Mineral	Cp	Cpx	Cpx	Cpx	Cpx	Cpx	Cpx3	Cpx	Cpx	Cpx	Cpx	Cpx	Cpx	Cpx	Cpx
Position	Core	Rim		Core	Rim	Core	Rim	Core	Rim		Core	Rim	Spongy	Core	Rim
Li	6.77	8.88	130	82.0	45.9	62.4	80.6	41.6	8.78	42.0	48.9	25.8	1.97	41.1	12.0
Sc	61.8	59.2	320	101	138	94.4	98.0	65.4	61.1	26.5	27.1	30.0	23.5	40.0	41.1
Ti	5000	5373	3661	3843	7798	2426	2836	2373	3119	5068	3677	4222	2976	1797	1942
V	151	151	1069	1655	1380	1520	1561	259	253	276	379	396	335	270	265
Cr	6041	5037	72,214	82,574	63,751	68,949	71,354	5384	5021	267	8276	8259	7906	10,075	9744
Mn	444	851	34,196	13,754	11,667	14,272	14,917	664	644	1002	749	769	703	661	676
Co	22.5	51.3	4217	962	769	884	939	20.7	22.5	45.2	30.6	28.4	26.2	25.5	22.6
Ni	258	589	86,117	13,936	16,462	13,209	13,524	358	338	344	508	430	454	441	374
Cu	7.88	27.1	242	91.3	1150	88.4	97.4	1.47	2.58	4.01	4.22	2.18	0.98	1.29	6.58
Rb	1.62	18.8	105	35.3	50.6	4.98	12.9	0.22	1.49	0.14	1.89	2.45	2.19	12.5	8.45
Sr	288	378	255	81.9	324	80.0	90.1	72.6	204	98.2	206	190	203	132	280
Y	9.80	10.8	12.2	2.59	14.5	1.87	2.43	15.0	15.7	7.20	3.85	8.47	3.53	4.11	5.14
Zr	68.9	86.6	56.6	16.1	110	16.4	19.3	26.0	44.7	27.6	23.4	30.9	16.4	28.3	21.1
Nb	7.69	8.56	11.9	4.40	22.0	3.78	4.84	0.28	3.65	0.18	1.52	1.21	0.72	6.37	2.83
Cs	0.05	2.49	19.3	2.06	3.71	0.71	1.26	0.09	0.10	0.03	0.07	0.21	0.09	0.04	0.56
Ba	40.0	213	1322	196	4086	115	299	1.16	101	138	3.99	6.97	49.3	12.4	18.5
La	8.76	10.7	9.69	3.27	10.2	3.40	4.53	1.02	7.49	1.74	3.35	6.61	3.04	3.41	8.09
Ce	22.3	26.1	15.5	7.06	19.9	6.55	8.46	3.37	18.7	6.42	17.9	25.0	14.8	12.2	21.7
Pr	3.17	3.63	1.48	0.77	2.52	0.79	0.99	0.58	2.51	1.15	3.23	4.21	2.69	2.18	3.17
Nd	16.2	17.7	7.05	3.10	8.58	2.90	3.65	3.68	10.8	6.72	15.3	20.4	13.2	11.7	14.7
Sm	3.72	4.34	1.75	0.76	1.93	0.85	1.00	1.41	2.62	2.15	3.18	4.36	2.98	3.20	3.81
Eu	1.24	1.39	0.69	0.24	0.87	0.23	0.25	0.63	1.15	0.77	0.99	1.40	0.81	0.99	1.40
Gd	3.19	3.36	2.44	0.72	2.04	0.68	1.07	1.93	2.71	2.05	1.98	3.25	1.66	2.10	2.43
Tb	0.46	0.47	0.32	0.10	0.34	0.11	0.13	0.39	0.49	0.33	0.26	0.43	0.21	0.26	0.31
Dy	2.29	2.57	2.01	0.66	2.10	0.59	0.73	2.53	3.09	1.76	1.10	2.02	0.96	1.14	1.27
Ho	0.43	0.45	0.48	0.13	0.46	0.12	0.16	0.56	0.64	0.31	0.18	0.36	0.16	0.18	0.22
Er	0.92	0.97	1.59	0.40	1.18	0.34	0.40	1.57	1.66	0.70	0.32	0.81	0.32	0.37	0.43
Tm	0.14	0.13	0.23	0.06	0.23	0.05	0.07	0.22	0.23	0.08	0.03	0.09	0.03	0.05	0.07
Yb	0.73	0.87	2.04	0.35	1.56	0.30	0.46	1.72	1.55	0.46	0.18	0.64	0.17	0.31	0.28
Lu	0.11	0.11	0.32	0.06	0.25	0.05	0.05	0.22	0.20	0.06	0.03	0.08	0.03	0.04	0.05
Hf	1.69	1.95	1.01	0.46	2.18	0.28	0.38	0.80	1.08	1.29	1.03	1.09	0.75	0.91	0.81
Ta	0.26	0.37	0.22	0.17	0.49	0.14	0.18	0.02	0.22	0.03	0.13	0.09	0.06	0.38	0.25
Pb	0.41	0.94	6.04	14.6	61.2	10.3	35.4	0.54	0.79	0.15	0.51	0.66	0.20	0.39	0.37
Th	0.46	0.74	0.48	0.43	5.92	0.28	0.53	0.03	0.28	0.02	0.24	0.14	0.07	0.92	0.33
U	0.15	0.11	0.26	0.21	2.16	0.18	0.32	0.01	0.08	0.00	0.06	0.03	0.03	0.24	0.08

Note: Analyses of minerals were carried out on a laser ablation microprobe coupled to an ICPMS (LA-ICPMS), at the State Key Laboratory of Lithospheric Evolution, Institute of Geology and Geophysics, Chinese Academy of Sciences. A spot size of 40 μm was used throughout this study. Helium was used as the carrier gas. External standard was NIST610, and internal standard was ^{42}Ca (for more analytical details, see Gao et al., 2002). CP, clinopyroxenite; CPM, clinopyroxene megacryst; GLH, garnet lherzolite; LH, lherzolite; SLH, spinel lherzolite; WH, wehrlite; Amph, amphibole; Cpx; clinopyroxene; Phl, phlogopite.

elements and isotopes (Yu et al., 2004; Mo et al., 2006; Dong et al., 2008). This oceanic-like thermal condition and OIB-like geochemistry of mantle-derived magmas suggest that the lithosphere beneath the Western Qinling preserved oceanic components. The Western Qinling was a suture zone evidenced by its outcropping ophiolites which is interpreted to be derived from subduction of ancient Tethys Ocean in the Cenozoic (Zhang and Zhou, 2001; Xu et al., 2002a,b). Therefore, the oceanic components preserved within the Western Qinling lithosphere are likely to be residual ancient Tethys oceanic material.

As shown in Fig. 8, lithospheric mantle exists to depths of at least 120 km beneath the Western Qinling and much thicker than that of Eastern China which is believed to have undergone large-scale thinning (e.g., Menzies et al., 1993; Fan et al., 2000; Zhang, 2005, 2006; Zhang et al., 2007a,b, 2008). Compared to the Tibetan Plateau and its adjacent regions, the depth of 120 km is common perhaps related to crustal thickening due to the distance effect of main collision zone (Gao et al., 1996; Zhou et al., 2000; Zhang et al., 2001, 2002a,b; Xu et al., 2002a,b). It therefore becomes apparent that the Western Qinling can be a very central study area in the effort to understanding the long-distance effects from Tibet, Eastern China and even the Pacific Ocean.

5.2. Mantle metasomatism agents

Mantle enrichment process has generally been attributed to metasomatism by silicate melts (e.g., Zangana et al., 1999), carbonatite melts (e.g., Thibault and Edgar, 1990; Rudnick et al., 1993; Yaxley et al., 1998; Hammouda and Laporte, 2000; Zheng et al., 2005) or CO_2–H_2O fluids (e.g., Ionov et al., 1997). All metasomatism agents produced strong mineral changes in mantle peridotites with an extensive formation of high-Cr clinopyroxene and conversion of harzburgite and dunite into lherzolite and wehrlite (e.g., Gasparik and Litvin, 2002; Shaw and Dingwell, 2008). The major element (especially Na) and trace element abundances, together with some ratios and anomalies in normalized diagram, have been used as indicators to identify mantle metasomatism. However, the discrimination of metasomatized types is problematic because the occurrences of alkali silicate metasomatism is universal and well documented (e.g., Zangana et al., 1999; Wulff-Pedersen et al., 1999), whereas carbonatite metasomatism are less common (Yaxley et al., 1991; Dautria et al., 1992; Rudnick et al., 1993; Ionov et al., 1995).

Xenoliths thought to be reaction products of a carbonatite melt display greater enrichments in REE and greater depletion in Ti and Zr than those thought to be metasomatized by silicate melts. TiO2 content of the carbonatite is very low but the fractionation between LREE and HREE is extremely high (Wallace and Green, 1988; Nelson et al., 1988). Therefore, the Ti/Eu together with $(La/Yb)_N$ ratios may be taken as indicators of carbonatite metasomatism, the Ti/Eu usually being <1500, whilst $(La/Yb)_N$ typically >3–4 (Rudnick et al., 1993; Klemme et al., 1995). Carbonatite melts are more enriched in highly incompatible elements, including U, Th, K, Cs, Rb, Ba and rare gases than silicate melts (Dasgupta and Hirschmann, 2006). The complexity is that any individual silicate or carbonatite metasomatism cannot

HT-14 CP		HT-15 SLH		HT-46 SLH		HT-16 SLH	HT-23 LH			HT-31 CPM	HT-35 LH			HT-44 CP		
Cpx	Cpx	Cpx	Cpx	Cpx	Phl	Cpx	Cpx	Cpx	Phl	Cpx	Cpx	Cpx	Amph	Cpx	Cp	Phl
Core	Rim	Core	Rim				Core	Rim			Core	Rim		Core	Rim	
1.12	1.29	14.3	17.9	30.2	6152	1396	15.1	11.9	32.6	456	0.90	1.39	7.09	24.7	19.7	0.02
94.1	81.4	270	266	35.6	20.1	447	76.7	76.0	0.13	327	20.5	31.4	0.76	45.3	45.4	0.85
16,513	17,112	1279	4668	478	2,211,608	8828	967	1021	18,127	55,121	1819	2883	155	103	153	26.2
120	130	1163	1206	179	4654	559	184	185	36.2	3511	289	358	4.65	218	219	5.03
3185	2123	89,855	87,757	8393	1847	40,150	5167	5714	17.5	3568	37.6	97.3	7.86	15,035	15,120	280
499	543	13,341	13,884	642	30,705	155,364	491	487	236	12,360	685	1036	55.3	719	722	5.06
25.4	26.4	859	897	27.2	3578	23,988	16.8	16.7	28.0	542	11.0	7.61	1.30	27.3	28.1	0.29
176	155	12,818	13,282	475	19,723	553,396	300	290	171	3914	20.4	3.22	3.73	462	508	3.88
1.23	1.25	44.0	126	2.08	249	888	1.51	2.69	2.13	49.0	0.91	4.00	7.50	1.75	12.0	0.05
0.17	0.13	9.66	74.2	0.33	18,084	34.6	0.09	0.14	122	2.04	0.37	2.23	29.7	0.10	0.55	0.50
280	315	61.3	286	134	2954	2279	79.9	93.2	119	539	465	421	41.9	34.4	62.2	29.2
16.8	18.9	3.51	7.15	3.56	31.1	26.2	5.94	6.27	1.15	93.0	5.91	13.9	3.35	0.86	0.93	0.00
269	278	11.2	57.6	16.7	443	153	20.4	21.3	7.44	297	151	156	74.0	6.10	7.07	0.05
1.92	1.95	2.33	15.6	0.93	2593	41.4	0.09	0.15	76.5	2.27	0.68	4.21	1.77	11.4	11.6	0.04
0.03	0.03	0.64	5.01	0.02	58.6	4.71	0.03	0.03	0.50	0.37	0.02	0.03	0.35	0.02	0.03	0.00
2.15	1.87	30.1	201	4.66	943,256	728	3.63	2.15	7393	1.03	9.12	35.7	54.3	0.28	5.90	1.32
14.4	15.9	1.44	10.8	2.06	48.6	109	1.98	3.96	4.32	20.5	7.41	19.1	6.17	1.54	1.78	0.01
42.2	45.8	2.86	21.4	7.15	71.8	182	6.04	9.37	6.67	68.8	17.6	54.6	11.0	2.98	3.46	0.03
6.55	7.22	0.34	2.35	1.09	8.01	19.9	0.94	1.26	0.66	11.9	2.34	7.74	1.16	0.28	0.34	0.00
34.9	38.9	1.54	8.99	5.24	22.6	65.7	5.03	6.08	2.53	70.7	10.9	32.8	4.36	0.99	1.15	0.01
8.86	9.70	0.58	2.34	1.43	4.82	11.1	1.45	1.62	0.46	22.9	2.27	6.09	0.59	0.27	0.30	0.00
2.80	3.09	0.17	0.71	0.46	4.72	3.43	0.47	0.46	0.14	8.66	0.91	1.62	0.15	0.11	0.13	0.00
7.11	8.18	0.56	2.12	1.13	6.01	14.3	1.38	1.35	0.66	24.1	1.54	4.44	0.58	0.24	0.28	0.00
0.94	1.07	0.09	0.23	0.15	0.69	2.07	0.20	0.23	0.05	3.80	0.24	0.65	0.09	0.04	0.04	0.00
4.52	5.07	0.48	1.40	0.77	3.75	7.46	1.24	1.29	0.21	21.7	1.22	3.49	0.69	0.18	0.21	0.00
0.72	0.80	0.11	0.23	0.15	0.74	1.37	0.25	0.25	0.04	3.87	0.23	0.64	0.14	0.03	0.04	0.00
1.51	1.65	0.35	0.87	0.34	2.14	2.88	0.65	0.69	0.09	8.59	0.61	1.60	0.31	0.09	0.10	0.00
0.17	0.18	0.05	0.12	0.05	0.38	0.53	0.09	0.09	0.01	1.07	0.10	0.25	0.05	0.01	0.02	0.00
1.02	1.18	0.34	0.84	0.31	2.49	3.84	0.60	0.66	0.07	6.25	0.66	1.73	0.27	0.10	0.11	0.00
0.12	0.14	0.05	0.14	0.05	0.27	0.52	0.08	0.09	0.01	0.75	0.10	0.27	0.04	0.01	0.02	0.00
10.6	10.5	0.17	1.34	0.44	7.55	2.67	0.76	0.77	0.15	14.2	5.25	4.18	1.96	0.05	0.07	0.00
0.35	0.37	0.08	0.57	0.10	62.3	1.27	0.01	0.01	4.39	0.32	0.02	0.16	0.12	1.71	1.72	0.00
0.08	0.11	9.36	2.98	0.61	59.6	45.3	0.17	0.18	0.14	0.52	0.27	0.76	6.16	1.21	1.25	0.02
0.22	0.24	0.20	1.30	0.08	0.52	8.91	0.22	0.26	0.14	0.28	0.02	0.42	2.77	4.97	5.06	0.00
0.02	0.02	0.11	0.27	0.03	1.35	2.58	0.01	0.04	0.11	0.06	0.02	0.08	1.10	1.13	1.14	0.00

interpret all the observed petrological, mineralogical and geochemical features. Thus, metasomatized melts may be a mixture of two melts with variable proportions.

Metasomatic signatures in the Western Qinling xenoliths include: (1) lherzolite-dominated, rare dunite and absence of harzburgite; (2) presence of phlogopite with high Ti, amphibole, calcite, ilmenite, apatite, barite, pyrite and observed zoning texture in pyroxene; (3) occurrence of discrete calcite grains associated with barite in contact with Ca-enriched orthopyroxene and olivine; (4) Cr, Na, LREE enrichment and Ti, Ba, Th, U, Sr, Pb, Zr, Hf, and Y anomalies in clinopyroxenes, particularly in their rims; (5) fractionation of LREE and HREE; (6) compositional variations between core and rim of pyroxenes. Ti/Eu and $(La/Yb)_N$ in the Western Qinling clinopyroxenes have large ranges of 902–15,813 and 0–20, respectively, and mostly plot outside of the defined world-wide silicate and carbonatite metasomatism fields (Fig. 9), suggesting single metasomatism agent from a mixed melt or two/multi metasomatism agents involving silicate and carbonatite. The compositional differences between core and rim of pyroxenes (Figs. 6 and 7) and large variations among samples reveal heterogeneously metasomatized by melts. The dissolution of orthopyroxene and growth of clinopyroxene (Figs. 2A, F and 3C, D) are consistent with the peridotite–melt reaction, which causes orthopyroxene melting and recrystallization of olivine and/or clinopyroxene (Shaw and Edgar, 1997; Franz and Wirth, 1997; Zhang et al., 2007a,b; Shaw and Dingwell, 2008). In the case of the Western Qinling xenoliths, the recrystallized olivine and clinopyroxene, especially in pockets have Mg# and CaO contents which are mostly higher than, or similar to those of the primary minerals (Table 2; Su et al., 2009). Lee et al. (2000) and Ionov and Harmer (2002) have concluded that carbonate grains and pockets in peridotites are crystal "cumulates" from carbonate-rich melts rather than quenched carbonatite liquids. The carbonate grains observed in the Baiguan xenoliths would be the direct evidence for carbonatite metasomatism.

To some extent, the Baiguan and Haoti xenoliths show different records. In the Baiguan xenoliths, the presence of calcite, barite, apatite and the positive anomalies in Ba, Th, U, Sr and Y in clinopyroxenes suggest carbonatite metasomatism, whereas the occurrence of ilmenite and a positive Ti anomaly in some samples could also reflect silicate–melt metasomatism (Neumann et al., 2002). In the Haoti peridotite, evidence of carbonatite metasomatism comes from the presence of low-Ti amphibole, CaO, Na_2O and TiO_2 variations in pyroxenes and/or olivines (Figs. 4 and 5), and some trace element abundances and ratios in clinopyroxenes and amphibole (Fig. 7). Although it is equally possible for Ti-poor amphibole to be deposited from hydrous fluids (Witt-Eickschen and Harte, 1994), this deposition cannot give reasonable interpretation to other trace elements in amphibole and particularly in clinopyroxene. The presence of phlogopite with high Ti (Fig. 7E), on the other hand, could indicate silicate metasomatism. These metasomatic agents could be interpreted as two/multi stage, based on the positive and negative anomalies in Ba, Pb, Ti etc. in both localities. Therefore, the Baiguan xenoliths have undergone modal carbonatite metasomatism and the Haoti xenoliths were mainly metasomatized by silicate melts and subsequently by weak carbonatite

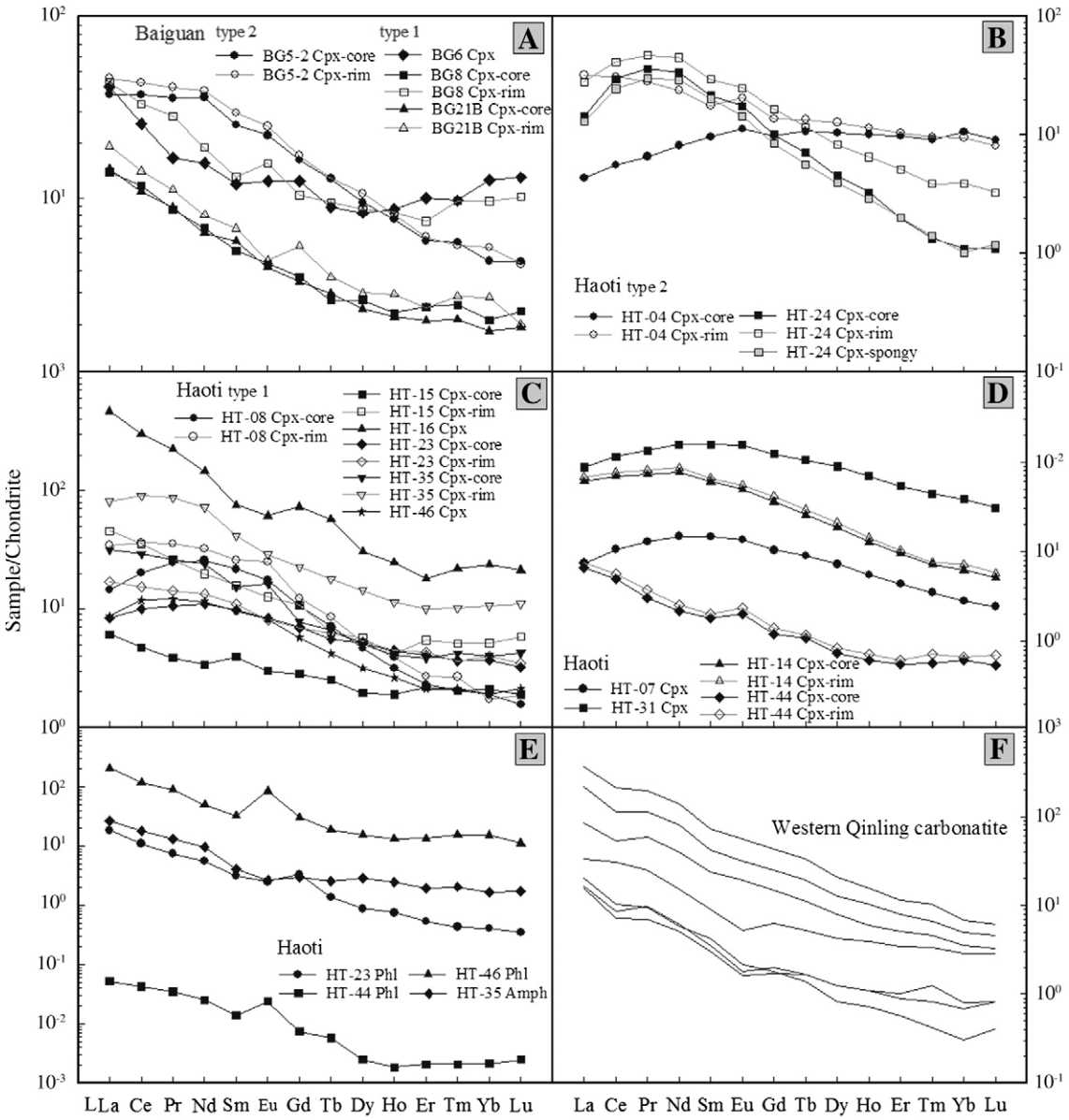

Fig. 6. Chondrite-normalized REE patterns of clinopyroxenes in the mantle xenoliths and carbonatites (from Yu et al., 2003) from the Western Qinling. Chondrite normalizing values from Anders and Grevesse (1989).

melts, which is evidenced by Ba, Th, U, and Sr depleted features for carbonatite metasomatism. If this inference is true, then Pb would be another indicator besides Ti, to distinguish carbonatite and silicate metasomatic agents. Carbonatite melts are rich in Ca besides CO_2 and H_2O, and therefore those elements, such as Pb, Sr, Ba, and Mg with similar chemical activities to Ca (Stracke and Bourdon, 2009; Dalou et al., 2009), would be concentrated in carbonatite melts. As shown in Fig. 7, Pb enrichment is clearly remarkable in Baiguan xenoliths but quite weak or depleted in Haoti xenoliths.

5.3. Origin of metasomatized melts

The silicate component is dominant in mantle melts and its origin has been well documented by several studies (e.g., Menzies and Hawkeworth, 1987; Coltorti et al., 1999; Gorring and Kay, 2000). In the current study, our discussion is focused on the possible source of carbonatite melts. Our knowledge of carbonatite metasomatism is still limited because this agent is less common in the upper mantle and the origin of the CO_2 and H_2O in the metasomatizing melts or fluids is still problematic. Nevertheless, two possible origins have been proposed: 1) recycled subducting slab and 2) deep mantle-derived melts. Zindler and Hart (1986) and Weaver (1991) suggested that carbonatite-rich metasomatizing agents originated from recycled crustal components in the convecting mantle, and may be correlated with OIB sources. Coltorti et al. (1999), Van Achterbergh et al. (2002) and Walter et al. (2008) also suggested that the carbonatite melts or fluids may have originated from recycled material in or, most probably, below the asthenospheric mantle, brought down in a subducting slab at a former convergent plate margin. On the other hand, based on extensive studies on carbonatites and carbonatite metasomatized peridotite xenolith, carbonatite melts is interpreted to be derived from deep source and/or related with carbonatites (Dautria et al., 1992; Rudnick et al., 1993; Harmer and Gittins, 1998; Chazot et al., 1994; Gasparik and Litvin, 2002; Gaillard et al., 2008).

Carbonatite melts that metasomatized the Western Qinling peridotites has enrichment in Ca, Mg, LILE (Ba, Th, U, Pb) and REE, and depletion in Ti and Zr. These compositional features are extremely consistent with the Western Qinling carbonatites (Fig. 7). In the Ti/Eu–$(La/Yb)_N$ plot (Fig. 9), the metasomatic agent seems to be related with the Western Qinling

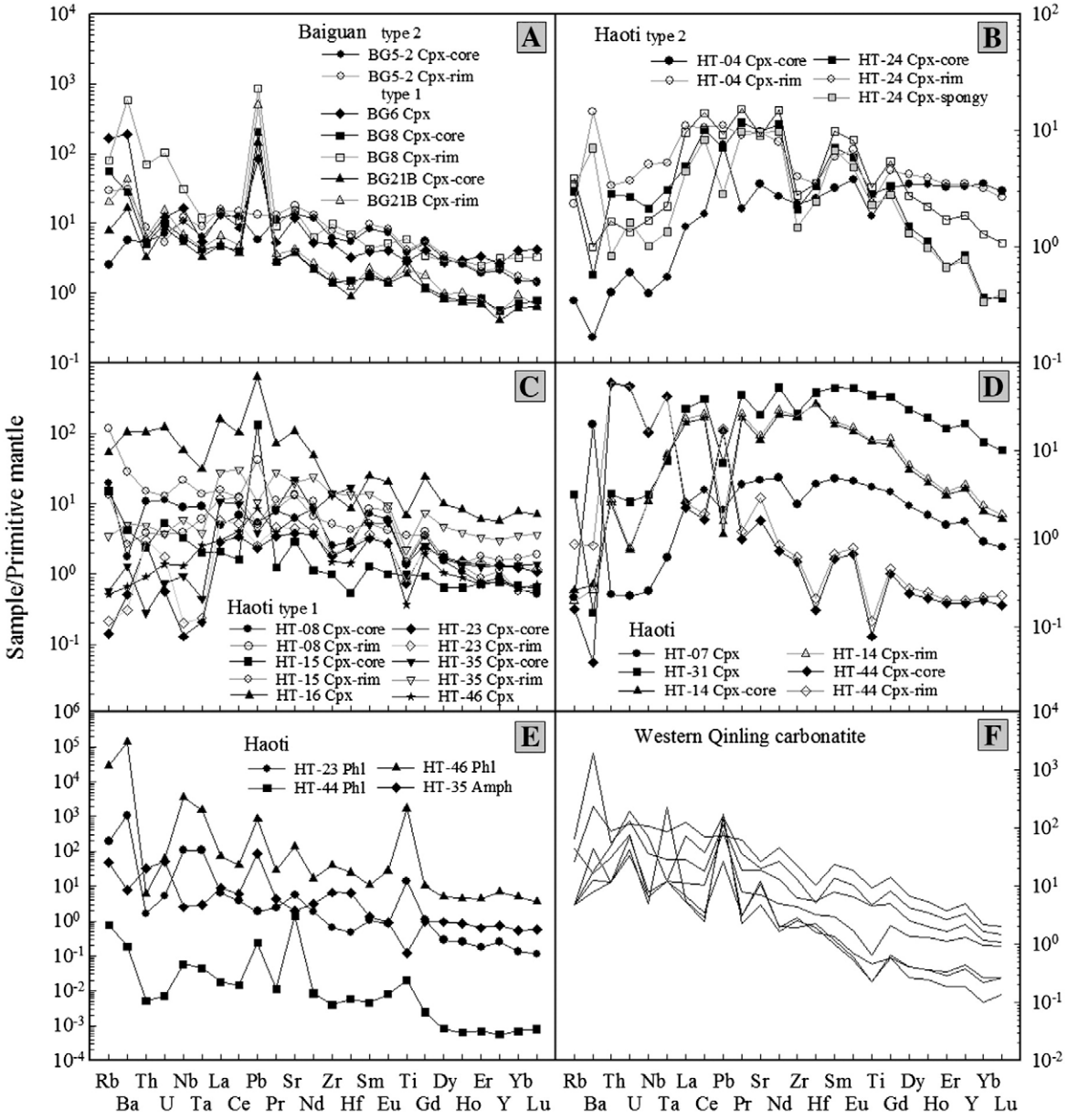

Fig. 7. Primitive mantle-normalized trace element patterns of clinopyroxenes in the mantle xenoliths and carbonatites (from Yu et al., 2003) from the Western Qinling. Primitive mantle normalizing values from Sun and McDonough, 1989.

carbonatite magma. The type 2 clinopyroxenes have similar Ti/Eu ratios to, and lower $(La/Yb)_N$ than those in carbonatites, and still show relative LILE and HFSE depletion and negative Ti and Pb anomalies (Fig. 7), indicating that this accretion of lithospheric mantle happened during, or mostly following carbonatite metasomatism.

Many experimental and geochemical studies indicated that carbonatite magmas are likely derived from depths in excess of 75 km (e.g., Thibault et al., 1992; Dalton and Wood, 1993; Harmer et al., 1998; Harmer and Gittins, 1998; Ying et al., 2004). Meanwhile, some researchers suggested that another possible source of primary carbonatite melts is deeply subducted oceanic crust, and that this type of carbonatite melts have higher Nd/Rb, intermediate La/Sm and lower Y/Nb compared to mid-ocean ridge basalts and primitive mantle (e.g., Walter et al., 2008). The Western Qinling carbonatites show much lower Nd/Rb, La/Sm and Y/Nb values than the carbonatites derived from subducted oceanic crust (Fig. 10), suggesting a different origin. La/Sm in the Western Qinling clinopyroxenes positively correlates with Nd/Rb and Y/Nb and the metasomatized trends evolve from depleted N-MORB to the Western Qinling carbonatites (Fig. 10). "Primary" carbonatite melts of subducted oceanic crust has higher La/Sm and Nd/Rb ratios, and contributes little or no material to metasomatic melts (e.g., Harmer and Gittins, 1998; Walter et al., 2008; Stracke and Bourdon, 2009), however, its contribution could be observed in the plot of La/Sm–Y/Nb. We, therefore, suggest that the origin of metasomatized carbonatite melts was mostly derived from deep mantle and probably related to carbonatite magmas, and that the contributions from subducted oceanic crust could not be completely excluded because the Western Qinling was formerly at a convergent plate margin in the Paleozoic and underwent subduction below the Tethyan Ocean in the Cenozoic (Gao et al., 1996; Zhou et al., 2000; Zhang et al., 2001, 2002a,b; Su et al., 2006b).

5.4. Petrogenesis of clinopyroxenite and clinopyroxene megacryst and formation of melt pocket

Clinopyroxene megacryst is generally believed to be high-pressure crystallization product of alkaline basaltic melts or accidentally-

Table 4
Estimated temperature (°C) and pressure (GPa) of mantle xenoliths from Baiguan, Lixian, Western Qinling.

Sample	*T* (W)	*T* (WB)	*T* (SS)	*T* (WS1)	*T* (WS2)	*T* (BK)	*P* (BK)
Type 1							
BG1	1174	1250	1174	1168	1067		
BG4	1182	1257					
BG5-1	1136	1212					
BG6	1197	1264				1216	3.44
BG8	1136	1210				1270	3.85
BG9	1195	1270	1344	1185	1006		
BG11	1164	1241	1153	973	1192		
BG21B	1126	1205					
BG21S	1205	1270					
BG23B	1174	1250					
BG23S	1170	1245					
BG24	1180	1213	1259	1913	1123		
Type 2							
BG5-2	781	903	890	841	892		

Note: *T* (W), Wells (1977), two-pyroxene thermometer; *T* (WB), Wood and Banno (1973), two-pyroxene thermometer; *T* (SS), Sachtleben and Seck (1981), Sp–Opx thermometer; *T* (WS1) and *T* (WS2), Witt and Seck (1991), Cr–Al–Opx thermometer and Sp–Opx thermometer; T(BK) and P (BK), Brey and Kohler (1990), Opx–Grt geothermobarometer.

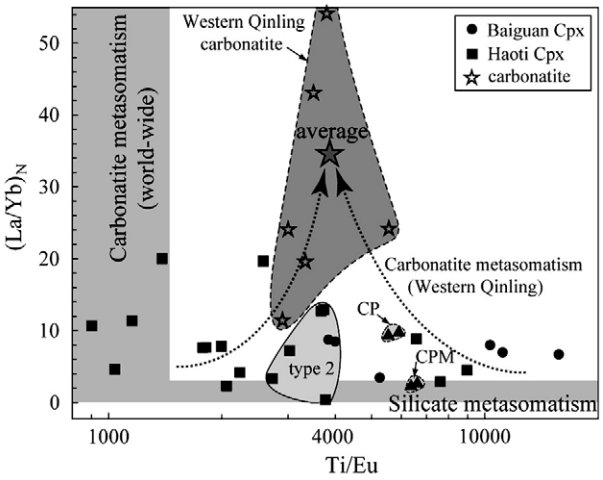

Fig. 9. Plot of Ti/Eu vs. $(La/Yb)_N$ of clinopyroxenes in mantle xenoliths and carbonatites (from Yu et al., 2003) from the Western Qinling. Grey fields of world-wide carbonatite and silicate metasomatism are after Rudnick et al. (1993). Dashed arrows indicate presumed carbonatite metasomatism in the Western Qinling peridotites.

included xenocryst of basaltic components (Xiao et al., 2008 and references therein). The clinopyroxenite (HT-14) has moderate trace element abundances and similar patterns to the megacrysts (HT-07 and HT-31), and thus is likely to be aggregation of clinopyroxene megacryst. These clinopyroxenes exhibit similar major element contents, REE abundances and convex-patterns to that of the type 2 clinopyroxenes, and also to the clinopyroxene megacrysts from Cenozoic basalts in North China Craton (Table 2; Fig. 6; Xiao et al.,

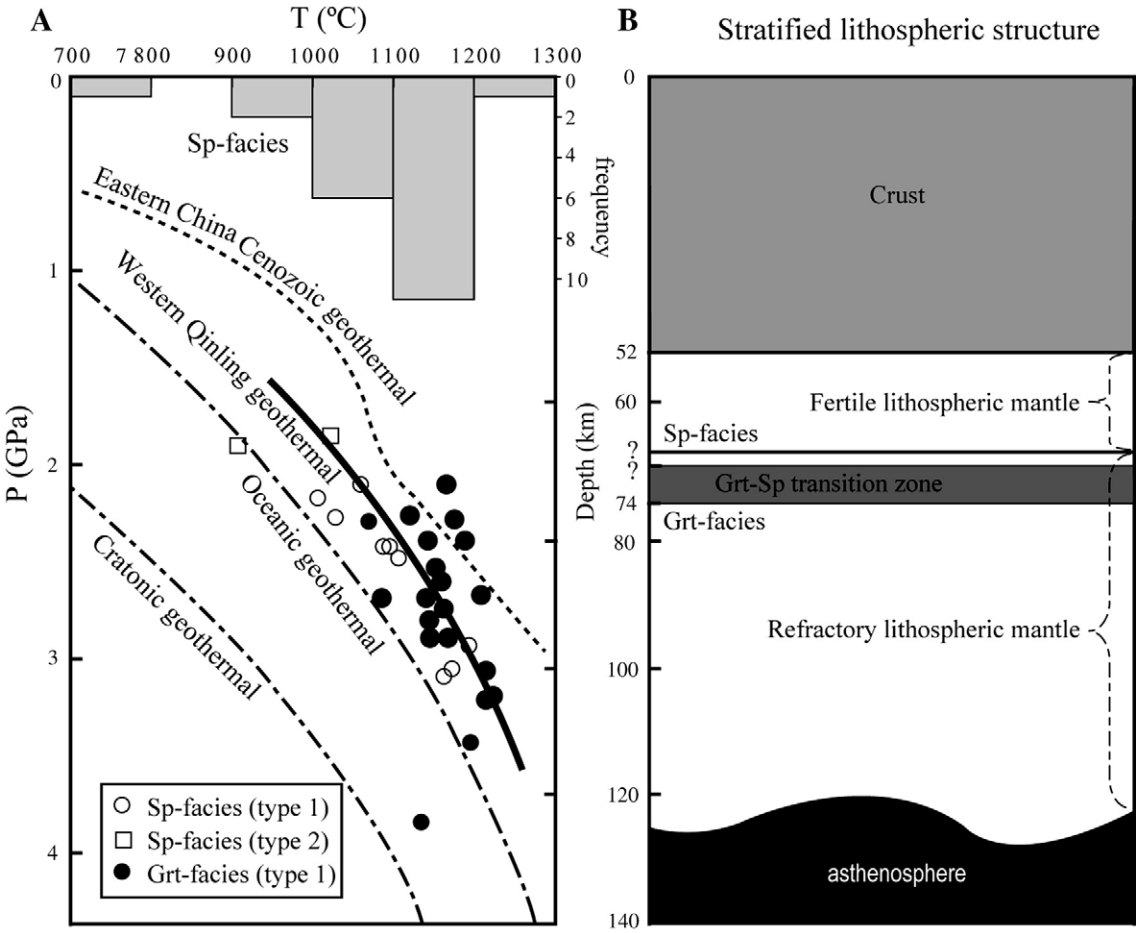

Fig. 8. A) Temperature–pressure estimates of the Western Qinling xenoliths. Data compiled from Yu et al. (2001), Shi et al. (2003), Su et al. (2007, 2009) and this study. Typical cratonic and oceanic geotherms are from Menzies and Chazot (1995); Eastern China Cenozoic geothermal is from Xu et al. (1995) and Su et al. (2007). Bold line is drawn on the basis of data distribution. Histogram in upper part denotes temperature estimates for spinel-facies and spinel-free peridotites. B) Schematic illustration of stratified lithospheric structure in the Western Qinling. Data except 52 km of crust from Li et al. (2002) and Shi et al. (2003) are based on this study.

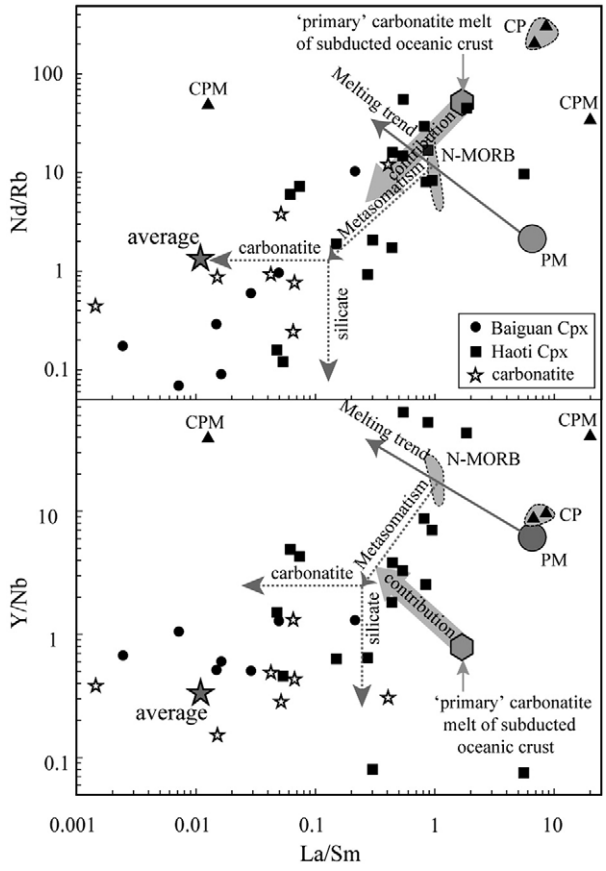

Fig. 10. Plots of Nd/Rb and Y/Nb against La/Sm of clinopyroxenes in mantle xenoliths and carbonatites (from Yu et al., 2003) from the Western Qinling. Grey line shows partial melting trend, and dashed grey lines show metasomatism trend. Grey-filled arrow represents contribution from "primary" carbonatite melts of subducted oceanic crust (from Walter et al., 2008). CP, clinopyroxenite; CPM, clinopyroxene megacryst; PM, primitive mantle (from Sun and McDonough, 1989); N-MORB, normal mid-oceanic ridge basalt (from Roux et al., 2002).

2008; Su et al., 2009), indicating similar petrogenesis. In primitive mantle-normalized spider diagram, these clinopyroxenes also show same patterns compared to the type 2 ones, but differ from the North China Craton clinopyroxenes in LILE, HFSE and Y (Fig. 7; Xiao et al., 2008), which may be caused by different primary melts (kamafugites and carbonatites in the Western Qinling; alkaline basalts in North China Craton). In Fig. 10, the clinopyroxenite and clinopyroxene megacrysts show no relationship with any metasomatic agent. Therefore, we suggest that the petrogenesis of the studied clinopyroxenite and clinopyroxene megacrysts is similar to that of world-wide clinopyroxenite/ clinopyroxene megacrysts, and crystallized simultaneously during the formation of the type 2 xenoliths.

Mantle carbonatite melts contains abundant volatile component (CO_2, H_2O, S, F, and Cl) and has low viscosity (0.36×10^{-3} PaS at 1.0 GPa, $T=1750$°K; Genge et al., 1995), and thus metasomatizes mantle peridotites mainly through infiltration and percolation (O'Reilly and Griffin, 1988; Ionov, 2001; Dalou et al., 2009). For mantle peridotite, triple junction between grains is the weakest position and could be easily eroded by reaction with melts. Emplacement of considerable quantities of melts would gradually react with contact minerals and produce mixed melts, followed by the formation of melt pocket, as long as there is no migration of melts. In most cases, the peridotite–melt reaction is expressed as: orthopyroxene + (Ca-enriched) melt = olivine + clinopyroxene ± glass/melt (Shaw and Edgar, 1997; Shaw et al., 2006; Zhang et al., 2007a,b; Shaw and Dingwell, 2008). The petrological observations in the Western Qinling xenoliths strongly confirm this observation (Figs. 2A, F and 3C, D). Again, if the reacting melt did not migrate, melt pocket could also form and relict orthopyroxene could sometimes be observed. If metasomatized peridotites with melt pocket were trapped by host magma and ascended to the Earth's surface rapidly, the melt pocket would be characterized by glass component as reported by Dawson (2002), which is interpreted as a quenching process and therefore lack time for crystallization. Given enough time, the melt in melt pocket would crystallize as olivine and clinopyroxene, and some accessory minerals such as calcite and barite as reported in Su et al. (2009) and this study.

5.5. Compositional stratification of lithospheric mantle beneath Western Qinling

Table 5 shows summaries of petrologic and geochemical features of two distinctive xenolith types from the Western Qinling. These summarized features indicate that the Western Qinling lithosphere, particularly beneath Baiguan and Haoti, is compositionally stratified. Refractory increases with temperature and pressure equivalent to depth (Figs. 4A, D and 8A). The shallower part of the lithospheric mantle is represented by type 2 xenoliths which lack alteration and deformation, and display fertile characteristics such as low Fo in olivine, Cr# in spinel and equilibrated temperature, and elevated Al_2O_3 and CaO in clinopyroxene, etc. (Fig. 4). These fertile peridotites are interpreted as growth of lithospheric mantle because they lack metasomatic signature (Su et al., 2009).

The dominant rock type is the refractory type 1 peridotites. The deeper part should have been involved in multiple and complex events. It is clear that these samples are refractory, having had more than 10% melt extraction from them (Su et al., 2009), and then underwent metasomatism as discussed above. The origin of this compositional stratification can be explained by the following possibilities: 1) stratification is a primary feature and represents a downward increase in the degree of partial melting. This possibility is consistent with asthenospheric upwelling (Yu et al., 2001, 2004; Su et al., 2006a, 2007, 2009) and the positive correlations of temperature/pressure and melting conditions (Figs. 4A, B, D and 8A). 2) Refertilization from a pre-existing depleted mantle section above possibly generated the stratification, but downward refertilization mechanisms and processes are unclear, although upward refertilization is conceivable (e.g., Lee and Rudnick, 1999; Tang et al., 2008). 3) Accretion of lithospheric mantle at the crust–mantle boundary may be the best interpretation. Most world-wide orogenic peridotites considered as exhumation from deep mantle are believed to form during orogenesis and post-orogenic movement. Mantle xenoliths entrained in Maguan (Yunnan, eastern Tibet) potassic basalts (11.75–13.3 Ma) were divided into two groups: fertile and refractory peridotites, and the fertile ones were considered to be newly-accreted

Table 5
Summarized features of two mantle xenolith types from the Western Qinling.

Type	Type 1	Type 2
Component	Spinel lherzolite, garnet lherzolite, wehrlite, websterite, dunite and clinopyroxenite	Spine lherzolite
Texture and deformation	Porphyroclastic texture, mineral elongation and orientation, strongly modified, melt pocket present	Fresh, fine-grained texture, mechanical comminution, weakly deformed, no melt pocket found
Olivine	High Fo > 90	Low Fo < 90
Clinopyroxene	Endiopside, low CaO ca. 20 wt.%, high Mg# and Cr#	diopside, high CaO > 20 wt.%, low Mg# and Cr#
Orthopyroxene	Low CaO and slightly low Al_2O_3	High CaO and slightly high Al_2O_3
Spinel	Fine grain, high-Cr# > 36	Coarse grain, low Cr# < 20
Garnet	Pyrope, breakdown texture	No garnet found
P–T	*P* up to 3.9 GPa, high *T* > 1100 °C	Low *T* < 1000 °C

based on major and trace elements and isotopes (Xia and Xu, 2006). In the case of the Western Qinling, it is tectonically located at a middle junction of east–west central orogen and north–south orogen in China and experienced the transition from oceanic (Tethys Ocean) to continental (present status) lithosphere during complex orogenic processes. Crustal-thickening due to uplift of Tibetan Plateau (Houseman and England, 1993; Jiang et al., 2006; Zhang et al., 2007a,b) has had an effect on the Western Qinling and should result in crust–mantle interaction. The peridotite xenoliths from the Western Qinling and Maguan (Yunnan) are comparable in petrology and mineral chemistry. The Western Qinling geotherm obtained from mainly refractory peridotites is parallel to the typical oceanic and continental geotherms, but is hotter than both (Fig. 8A), suggesting that these refractory peridotites preserve imprint of ancient oceanic lithosphere.

The garnet–spinel transition zone within the Western Qinling lithospheric mantle has a lower limit of 78 km (Su et al., 2007) and a potential upper limit of 65 to 70 km corresponding to the lowest limit of spinel-phase peridotite. The total thickness of the lithosphere is ca. 120 km (Fig. 8). Shi et al. (2003) suggested that the crust–mantle boundary beneath the Western Qinling is seated at a depth of 52 km. A recent seismic tomographic study revealed that the Western Qinling crust has upper and middle parts with thickness of 20 km and 10 km, respectively (Li et al., 2002). On the basis of the above discussion, the stratified lithospheric section beneath the Western Qinling is illustrated in Fig. 8B.

5.6. Significances on the lithosphere of orogenic belt

The heterogeneity of the Earth's mantle has been documented by several comprehensive studies (e.g., Hart, 1988; Hofmann, 2003; Zhang et al., 2004). In particular, large-scale heterogeneity involving one tectonic unit or the whole mantle, just like local compositional homogeneity of mantle, is largely accepted by most scientists (e.g., Morgan and Morgan, 1999). However, we strongly believe that small-scale heterogeneity should exist somewhere, e.g. the Eifel volcanic field in Germany (Witt-Eickschen and Harte, 1994; Witt-Eickschen et al., 1998; Shaw et al., 2005), though not everywhere within the mantle. The excellent targets for the small-scale heterogeneity should include the Western Qinling orogen where two localities, Baiguan and Haoti, crop out xenoliths with some distinctive features. On the whole, the Baiguan xenoliths are unitary in category restricted in lherzolite and dunite, and generally exhibit alteration and carbonatite metasomatism (Table 1; Figs. 3, 6 and 7), while the Haoti xenoliths consist of diverse peridotites extending from lherzolite, wehrlite to dunite, websterite, clinopyroxenite and even clinopyroxene megacryst, and have the presence of hydrous minerals, such as phlogopite and amphibole, instead of Ca-rich minerals (Su et al., 2009). In mineral chemistry, the Baiguan xenoliths have slightly higher Fo in olivine, Cr# in spinel, CaO in orthopyroxene and high equilibrated temperature and larger variation of Na_2O in clinopyroxene than the Haoti peridotites (Fig. 4), and are recording carbonatite metasomatism. Therefore, heterogeneity in petrology, mineralogy and geochemistry essentially exists within the lithospheric mantle beneath the Western Qinling.

The lithosphere beneath the Western Qinling, represented by the type 2 xenolith has newly-accreted and fertile features and is seated around the crust–mantle boundary (Fig. 5A). Therefore, we propose that the shallower lithospheric mantle was most likely generated from the crust–mantle interaction during formation of an orogenic belt. The Dabie–Sulu and Eastern Alps orogens have revealed crocodile-like subduction and collision structure (Li, 1994; Lin, 1995; Xu et al., 2001, 2002a,b; TRANSALP Working Group, 2002), which are excellent tectonic settings for crust–mantle interaction. Moreover, exposed garnet peridotite massifs within orogenic belts are assumed to be exhumed from ancient slab subducted to great depths sometimes up to 300 km (Van Roermund and Drury, 1998; Ye et al., 2000; Van Roermund et al., 2001), though the mechanism involved has not been solved yet. Tectonic, geochemical and geochronological comparisons between orogenic garnet peridotite massif and garnet peridotite xenolith imply that the mixing and interaction of crustal and mantle materials are the key processes responsible for generating orogenic peridotite. Although orogenic peridotite massif and lenses have been discovered in many localities and been studied in more detail, mantle xenoliths from orogenic belts are rarely reported, perhaps because long-time intensive setting doesn't allow eruption of xenolith-bearing volcanic rocks. Therefore, Western Qinling and its outcropping mantle xenoliths should be an important locality and target to investigate the complex evolution history of orogenic belts.

6. Conclusions

1) The lithosphere beneath the Western Qinling is geothermally hotter than typical cratonic and oceanic environments, and has the thickness of ca. 120 km and a compositionally stratified structure with a step-wise decrease in fertility with depth.
2) In-situ trace element data for clinopyroxenes, phlogopites and amphibole in the Western Qinling xenoliths show complex variations between both localities and both types. Combining petrological features and distributions of REE, LILE, HFSE, we conclude that at least two episodes of metasomatism occurred, and that carbonatite metasomatism was predominant in Baiguan but less dominant in Haoti.
3) Comparisons with the Western Qinling carbonatites and world-wide carbonatite melts indicate that carbonatite melts involving in metasomatism originated from deep mantle and most likely related to carbonatite magma, with some contributions from subducted oceanic crust.

Acknowledgements

This research was financially supported by the Knowledge Innovation Program of the Chinese Academy of Sciences (Grant KZCX2-YW-103), the National Science Foundation of China (Grants, 90714008, and 40721062) and the grant from the University of Hong Kong. The authors would like to extend their sincere gratitude to Q. Mao and Y.G. Ma for their assistance in major elements analyses at the State Key Laboratory of Lithospheric Evolution of the Institute of Geology and Geophysics, and also thank Dr. Benny Chisonga for improving the original manuscript. We gratefully acknowledge the editor and two anonymous reviewers for editorial handling and helpful comments.

Appendix A. Supplementary data

Supplementary data associated with this article can be found, in the online version, at doi:10.1016/j.tecto.2010.01.005.

References

Anders, E., Grevesse, N., 1989. Abundances of the elements: meteoritic and solar. Geochimica et Cosmochimica Acta 53, 197–214.
Boyd, F.R., 1989. Composition and distinction between oceanic and cratonic lithosphere. Earth and Planetary Science Letters 96, 15–26.
Brey, G.P., Kohler, T., 1990. Geothermobarometry in four-phase lherzolites II, new thermobarometers and practical assessment of existing thermobarometers. Journal of Petrology 31, 1353–1378.
Canil, D., 1991. Experimental study bearing on the absence of carbonate in mantle derived xenoliths. Geology 18, 1011–1013.
Chazot, G., Menzies, M.A., Harte, B., Mattey, D., 1994. Carbonatite metasomatism and melting of the Arabian lithosphere: evidence from oxygen isotopes and trace element composition of spinel lherzolites. Mineralogical Magazine 58A, 167–168.
Coltorti, M., Bonadiman, C., Hinton, R.W., Siena, F., Upton, B.G., 1999. Carbonatite metasomatism of the ocean upper mantle: evidence from clinopyroxenes and glasses in ultra-mafic xenoliths of Grande Comore, Indian Ocean. Journal of Petrology 40, 133–165.

Dalou, C., Koga, K.T., Hammouda, T., Poitrasson, F., 2009. Trace element partitioning between carbonatitic melts and mantle transition zone minerals: implications for the source of carbonatites. Geochimica et Cosmochimica Acta 73, 239–255.
Dalton, J.A., Wood, B.J., 1993. The composition of primary carbonate melts and their evolution through wallrock reaction in the mantle. Earth and Planetary Science Letters 119, 511–525.
Dasgupta, R., Hirschmann, M.M., 2006. Melting in the Earth's deep upper mantle caused by carbon dioxide. Nature 440, 659–662.
Dautria, J.M., Dupuy, C., Takherist, D., Dostal, J., 1992. Carbonate metasomatism in the lithospheric mantle: peridotitic xenoliths from a melilititic district of the Sahara basin. Contributions to Mineralogy and Petrology 111, 37–52.
Dawson, J.B., 2002. Metasomatism and partial melting in upper-mantle peridotite xenoliths from the Lashaine volcano, Northern Tanzania. Journal of Petrology 43, 1749–1777.
Dong, X., Zhao, Z.D., Mo, X.X., Yu, X.H., Zhang, H.F., Li, B., Depaolo, D.J., 2008. Geochemistry of the Cenozoic kamfugites from west Qinling and its constraint for the nature of magma source region. Acta Petrologica Sinica 24, 238–248 (in Chinese with English abstract).
Downes, H., 2001. Formation and modification of the shallow sub-continental lithospheric mantle: a review of geochemical evidence from ultramafic xenolith suites and tectonically emplaced ultramafic massifs of western and central Europe. Journal of Petrology 42, 233–250.
Downes, H., Beard, A., Hinton, R., 2004. Natural experimental charges: an ion-microprobe study of trace element distribution coefficients in glass-rich hornblendite and clinopyroxenite xenoliths. Lithos 75, 1–17.
Fan, W.M., Zhang, H.F., Baker, J., Jarvis, K.E., Mason, P.R.D., Menzies, M.A., 2000. On and off the North China Craton: where is the Archean Keel? Journal of Petrology 41, 933–950.
Francis, D., Patterson, M., 2009. Kimberlites and aillikites as probes of the continental lithospheric mantle. Lithos 109, 72–80.
Franz, L., Wirth, R., 1997. Thin intergranular melt films and melt pockets in spinel peridotite xenoliths from the Rhon area (Germany): early stage of melt generation by grain boundary melting. Contributions to Mineralogy and Petrology 129, 268–283.
Gaillard, F., Malki, M., Lacono-Marziano, G., Pichavant, M., Scaillet, B., 2008. Carbonatite melts and electrical conductivity in the asthenosphere. Science 322, 1363–1365.
Gao, S., Zhang, B.R., Wang, D.P., Ouyang, J.P., Xie, Q.L., 1996. Geochemical evidence for the Proterozoic tectonic evolution of the Qinling Orogenic Belt and its adjacent margins of the North China and Yangtze cratons. Precambrian Research 80, 23–48.
Gao, S., Liu, X., Yuan, H., Hattendorf, B., Günther, D., Chen, L., Hu, S., 2002. Analysis of forty-two major and trace elements of USGS and NIST SRM glasses by LA-ICPMS. Geostandards and Geoanalytical Research 26, 181–196.
Gasparik, T., Litvin, Y.A., 2002. Experimental investigation of the effect of metasomatism by carbonatic melt on the composition and structure of the deep mantle. Lithos 60, 129–143.
Genge, M.J., Price, G.D., Jones, A.P., 1995. Molecular dynamics simulations of $CaCO_3$ melts to mantle pressures and temperatures: implications for carbonatite magmas. Earth and Planetary Science Letters 131, 225–238.
Gorring, M.L., Kay, S.M., 2000. Carbonatite metasomatized peridotite xenoliths from southern Patagonia: implications for lithospheric processes and Neogene plateau magmatism. Contributions to Mineralogy and Petrology 140, 55–72.
Green, D.H., Wallace, M.E., 1988. Mantle metasomatism by ephemeral carbonatite melts. Nature 336, 459–462.
Hammouda, T., 2003. High-pressure melting of carbonated eclogite and experimental constraints on carbon recycling and storage in the mantle. Earth and Planetary Science Letters 214, 357–368.
Hammouda, T., Laporte, D., 2000. Ultrafast mantle impregnation by carbonatite melts. Geology 28, 283–285.
Harmer, R.E., Gittins, J., 1998. The case for primary, mantle-derived carbonatite magma. Journal of Petrology 39, 1895–1903.
Harmer, R.E., Lee, C.A., Eglington, B.M., 1998. A deep mantle source for carbonatite magmatism: evidence from the nephelinites and carbonatites of the Buhera district, SE Zimbabwe. Earth and Planetary Science Letters 158, 131–142.
Hart, S.R., 1988. Heterogeneous mantle domains: signatures, genesis and mixing chronologies. Earth and Planetary Science Letters 90, 273–296.
Hofmann, A.W., 2003. Sampling mantle heterogeneity through oceanic basalts: isotopes and trace elements. Treaties on Geochemistry 2, 61–101.
Houseman, G., England, C., 1993. Crustal thickening versus lateral expulsion in the India–Asian continental collision. Journal of Geopgysical Research 98, 12233–12249.
Ionov, D.A., 2001. Carbonates in mantle xenoliths: quenched melts or crystal cumulates? Journal of African Earth Sciences 32, A19.
Ionov, D.A., Harmer, R.E., 2002. Trace element distribution in calcite–dolomite carbonatites from Spitskop: inferences for differentiation of carbonatite magmas and the origin of carbonates in mantle xenoliths. Earth and Planetary Science Letters 131, 341–356.
Ionov, D.A., Prikhod'ko, V.S., O'Reilly, S.Y., 1995. Peridotite xenoliths in alkali basalts from the Sikhote–Alin, southeastern Siberia, Russia: trace element signatures of mantle beneath a convergent continental margin. Chemical Geology 120, 275–294.
Ionov, D.A., O'Reilly, S.Y., Griffin, W.L., 1997. Volatile-bearing minerals and lithophile trace elements in the upper mantle. Chemical Geology 141, 153–184.
Ionov, D.A., Chazot, G., Chauvel, C., Merlet, C., Bodinier, J.L., 2006. Trace element distribution in peridotite xenoliths from Tok, SE Siberian craton: a record of pervasive, multi-stage metasomatism in shallow refractory mantle. Geochimica et Cosmochimica Acta 70, 1231–1260.
Jiang, M., Galvé, A., Hirn, A., Voogd, B., Laigle, M., Su, H.P., Diaz, J., Lépine, J.C., Wang, Y.X., 2006. Crustal thickening and variations in architecture from the Qaidam basin to the Qiangtang (North-Central Tibetan Plateau) from wide-angle reflection seismology. Tectonophysics 412, 121–140.
Klemme, S., van der Laan, S.R., Foley, S.F., Gunther, D., 1995. Experimentally determined trace and minor element partitioning between clinopyroxene and carbonatite melt under upper mantle conditions. Earth and Planetary Science Letters 133, 439–448.
Kohler, T.P., Brey, G.P., 1990. Calcium exchange between olivine and clinopyroxene calibrated as a geobarometer for natural peridotites from 2 to 60 kbar with applications. Geochimica et Cosmochimica Acta 54, 2375–2388.
Laurora, A., Mazzucchelli, M., Rivalenti, G., Vannucci, R., 2001. Metasomatism and melting in carbonated peridotite xenoliths from the mantle wedge: the Gobernador Gregores case (Southern Patagonia). Journal of Petrology 42, 69–87.
Lee, C.T., Rudnick, R.L., 1999. Compositionally stratified cratonic lithosphere: petrology and geochemistry of peridotite xenoliths from the Labait tuff cone, Tanzania. In: Gurney, J.J., Richardson, S.R. (Eds.), Proceedings of the 7th International Kimberlite Conference, pp. 503–521.
Lee, C.T., Rudnick, R.L., McDonough, W.F., Horn, I., 2000. Petrologic and geochemical investigation of carbonates in peridotite xenoliths from northeastern Tanzania. Contributions to Mineralogy and Petrology 139, 470–484.
Li, Z.X., 1994. Collision between the North and South China blocks: a crustal-detachment model for suturing in the region east of the Tanlu fault. Geology 22, 739–742.
Li, S.L., Zhang, X.K., Zhang, C.K., Zhao, J.R., Cheng, S.X., 2002. A preliminary study on the crustal velocity structure of Maqin–Lanzhou–Jingbian by means of deep seismic sounding profile. Chinese Journal of Geophysics 45, 210–217 (in Chinese with English abstract).
Lin, S.F., 1995. Collision between the North and South China blocks: a crustal-detachment model for suturing in the region east of the Tanlu fault: comment. Geology 23, 574–575.
Lloyd, F.E., 1987. Characterization of mantle metasomatic fluids in spinel lherzolite and alkali clinopyroxenites from the West Eifel and Uganda. In: Menzies, M.A., Hawkesworth, C.J. (Eds.), Mantle Metasomatism. Academic Press, pp. 91–123.
Mao, J.W., Qiu, Y.M., Goldfarb, R.J., Zhang, Z.C., Garwin, S., Ren, F.S., 2002. Geology, distribution, and classification of gold deposits in the western Qinling belt, central China. Mineralium Deposita 37, 352–377.
Menzies, M.A., Chazot, G., 1995. Fluid processes in diamond to spinel facies shallow mantle. Journal of Geodynamics 20, 387–415.
Menzies, M.A., Hawkeworth, C.J., 1987. Mantle Metasomatism. Academic Press, London. 472.
Menzies, M.A., Fan, W.M., Zhang, M., 1993. Paleozoic and Cenozoic lithoprobes and the loss of >120 km of Archean lithosphere, Sino–Korean craton, China. In: Prichard, H. M., Alabaster, T., Harris, N.B.W., Neary, C.R. (Eds.), Magmatic Processes and Plate Tectonics, vol. 76, pp. 71–81.
Mo, X.X., Zhao, Z.D., Deng, J.F., Flower, M., Yu, X.H., Luo, Z.H., Li, Y.G., Zhou, S., Dong, G.C., Zhu, D.C., Wang, L.L., 2006. Petrology and geochemistry of postcollisional volcanic rocks from the Tibetan plateau: implications for lithosphere heterogeneity and collision-induced asthenospheric mantle flow. Special Paper, Postcollisional Tectonics and Magmatism in the Mediterranean Region and Asia 409, 507–530.
Morgan, J.P., Morgan, W.J., 1999. Two-stage melting and the geochemical evolution of the mantle: a recipe for mantle plum-pudding. Earth and Planetary Science Letters 170, 215–239.
Nelson, D.R., Chivas, A.R., Chapell, B.W., McCulloch, M.T., 1988. Geochemical and isotopic systematics in carbonatites and implications for the evaluation of ocean-island sources. Geochimica et Cosmochimica Acta 52, 1–17.
Neumann, E.R., Wulff-Pedersen, E., Pearson, N.J., Spenser, E.A., 2002. Mantle xenoliths from Tenerife (Canary Islands): evidence for reactions between mantle peridotites and silicic carbonatite melts inducing Ca metasomatism. Journal of Petrology 43, 825–857.
O'Reilly, S.Y., Griffin, W.L., 1988. Mantle metasomatism beneath western Victoria, Australia: I. metasomatic processes in Cr-diopside lherzolites. Geochimica et Cosmochimica Acta 52, 433–448.
Pearson, D.G., Canil, D., Shirey, S.B., 2003. Mantle Samples included in volcanic rocks: xenoliths and diamonds. In: Holland, H.D., Turekin, K.K. (Eds.), Treatise of Geochemistry. Elsevier, Oxford, pp. 171–275.
Rosatellia, G., Wall, F., Stoppa, F., 2007. Calcio-carbonatite melts and metasomatism in the mantle beneath Mt. Vulture (Southern Italy). Lithos 99, 229–248.
Roux, P.J., Roex, A.P., Schilling, J.G., Shimizu, N., Perkins, W.W., Pearce, N.J.G., 2002. Mantle heterogeneity beneath the southern Mid-Atlantic Ridge: trace element evidence for contamination of ambient asthenospheric mantle. Earth and Planetary Science Letters 203, 479–498.
Rudnick, L.R., McDonough, W.F., Chappell, B.W., 1993. Carbonatite metasomatism in the northern Tanzanian mantle: petrographic and geochemical characteristics. Earth and Planetary Science Letters 114, 463–475.
Sachtleben, T.H., Seck, H.A., 1981. Chemical control of Al-solubility in orthopyroxene and its implications on pyroxene geothermometry. Contributions to Mineralogy and Petrology 78, 157–165.
Shaw, C.S.J., Dingwell, D.B., 2008. Experimental peridotite–melt reaction at one atmosphere: a textural and chemical study. Contributions to Mineralogy and Petrology 155, 199–214.
Shaw, C.S.J., Edgar, A.D., 1997. Post-entrainment mineral–melt reactions in spinel peridotite xenoliths from Inver, Donegal, Ireland. Geology Magazine 134, 771–779.
Shaw, C.S.J., Eyzaguirre, J., Fryer, B., Gagnon, J., 2005. Regional variations in the mineralogy of metasomatic assemblages in mantle xenoliths from the West Eifel volcanic field, Germany. Journal of Petrology 46, 945–972.
Shaw, C.S.J., Heidelbach, F., Dingwell, D.B., 2006. The origin of reaction textures in mantle peridotite xenoliths from Sal Island, Cape Verde: the case for "metasomatism" by the host lava. Contributions to Mineralogy and Petrology 151, 681–697.
Shi, L.B., Lin, C.Y., Chen, X.D., 2003. Composition, thermal structures and rheology of the upper mantle inferred from mantle xenoliths from Haoti, Dangchang, Gansu

Province, western China. Seismology and Geology 4, 525–542 (in Chinese with English abstract).
Stracke, A., Bourdon, B., 2009. The importance of melt extraction for tracing mantle heterogeneity. Geochimica et Cosmochimica Acta 73, 218–238.
Su, B.X., Chen, Y.L., Liu, F., Wang, Q.Y., Zhang, H.F., Lan, Z.W., 2006a. Geochemical characteristics and significance of Triassic sandstones of Songpan–Ganze block. Acta Petrologica Sinica 22, 961–970 (in Chinese with English abstract).
Su, B.X., Zhang, H.F., Xiao, Y., Zhao, X.M., 2006b. Characteristics and geological significance of olivine xenocrysts in Cenozoic volcanic rocks from western Qinling. Progress in Natural Science 16, 1300–1306.
Su, B.X., Zhang, H.F., Wang, Q.Y., Sun, H., Xiao, Y., Ying, J.F., 2007. Spinel–garnet phase transition zone of Cenozoic lithospheric mantle beneath the eastern China and western Qinling and its T–P conditions. Acta Petrologica Sinica 23, 1313–1320 (in Chinese with English abstract).
Su, B.X., Zhang, H.F., Ying, J.F., Xiao, Y., Zhao, X.M., 2009. Nature and processes of the lithospheric mantle beneath the western Qinling: evidence from deformed peridotitic xenoliths in Cenozoic kamafugite from Haoti, Gansu Province, China. Journal of Asian Earth Sciences 34, 258–274.
Sun, S.S., McDonough, W.F., 1989. Chemical and isotopic systematic of oceanic basalt: implication for mantle composition and processes. In: Saunders, A.D., Norry, M.J. (Eds.), Magmatism in the oceanic basins: Special Publication of Geological Society of London, vol. 42, pp. 313–346.
Tang, Y.J., Zhang, H.F., Ying, J.F., Zhang, J., Liu, X.M., 2008. Refertilization of ancient lithospheric mantle beneath the central North China Craton: evidence from petrology and geochemistry of peridotite xenoliths. Lithos 101, 435–452.
Thibault, Y., Edgar, A.D., 1990. Patent mantle-metasomatism: inferences based on experimental studies. Proceed of Indian Academy of Sciences 99, 21–37.
Thibault, Y., Edgar, A.D., Lloyd, F.E., 1992. Experimental investigation of melts from a carbonated phlogopite lherzolite: implications for metasomatism in the continental lithospheric mantle. American Mineralogist 77, 784–794.
Van Achterbergh, E., Griffin, W.L., Ryan, C.G., O'Reilly, S.Y., Pearson, N.J., Kivi, K., Doyle, B.J., 2002. Subduction signature for quenched carbonatites from the deep lithosphere. Geology 30, 743–746.
Van Roermund, H.L.M., Drury, M.R., 1998. Ultra-high pressure (P>6 GPa) garnet peridotites in western Norway: exhumation of mantle rocks from more than 185 km. Terra Nova 10, 295–301.
Van Roermund, H.L.M., Drury, M.R., Barnhoorn, A., Ronde, A.D., 2001. Relict majoritic garnet microstructures from ultra-deep orogenic peridotites in Western Norway. Journal of Petrology 42, 117–130.
Wallace, M.E., Green, D.H., 1988. Mantle metasomatism by ephemeral carbonatite melts. Nature 336, 459–462.
Walter, M.J., Bulanova, G.P., Armstrong, L.S., Keshav, S., Blundy, J.D., Gudfinnsson, G., Lord, O.T., Lennie, A.R., Clark, S.M., Smith, C.B., Gobbo, L., 2008. Primary carbonatite melt from deeply subducted oceanic crust. Nature 454, 622–626.
Wang, J., Li, J.P., Wang, J.H., Ma, Z.H., 2002. Geological implications for the mafic enclaves of deep derivation from Cenozoic shoshonitic rocks in Jianchuan–Dali area, western Yunnan. Acta Mineralogica Sinica 22, 113–125.
Weaver, B.L., 1991. The origin of ocean island basalt end-member compositions: trace element and isotopic constraints. Earth and Planetary Science Letters 104, 381–397.
Wells, P.R.A., 1977. Pyroxene thermometry in simple and complex systems. Contributions to Mineralogy and Petrology 62, 129–139.
Witt, G.E., Seck, H.A., 1991. Solubility of Ca and Al in orthopyroxene from spinel peridotite: an improved version of an empirical geothermometer. Contributions to Mineralogy and Petrology 106, 431–439.
Witt-Eickschen, G., Harte, B., 1994. Distribution of trace elements between amphibole and clinopyroxene from mantle peridotites of the Eifel (western Germany): an ion-microprobe study. Chemical Geology 117, 235–250.
Witt-Eickschen, G., Kaminsky, W., Kramm, U., Harte, B., 1998. The nature of young vein metasomatism in the lithosphere of the West Eifel (Germany): geochemical and isotopic constraints from composite mantle xenoliths from the Meerfelder Maar. Journal of Petrology 39, 155–185.
Wood, B.J., Banno, S., 1973. Garnet–orthopyroxene relationships in simple and complex systems. Contributions to Mineralogy and Petrology 42, 109–124.
Working Group, T.R.A.N.S.A.L.P., 2002. First deep seismic reflection images of the Eastern Alps reveal giant crustal wedges and transcrustal ramps. Geophysical Research Letters 29. doi:10.1029/2002GL014911.
Wulff-Pedersen, E., Neumann, E.R., Vannucci, R., Botazzi, P., Ottolini, L., 1999. Silicic melts produced by reaction between peridotite and infiltrating basaltic melts: ion probe data on glasses and minerals in veined xenoliths from La Palma, Canary Islands. Contributions to Mineralogy and Petrology 137, 59–82.
Wyllie, P.J., 1989. Origin of carbonatites: evidence from phase equilibrium studies. In: Bell, K. (Ed.), Carbonatites: Genesis and Evolution. Unwin Hyman, London, Boston, pp. 500–545.
Xia, P., Xu, Y.G., 2006. Mantle-derived xenoliths in Maguan Cenozoic potassic basalt, southeast Yunnan and its bearing on lithospheric composition and dynamics. Geochimica (Beijing) 35, 1–5 (in Chinese with English abstract).
Xiao, Y., Zhang, H.F., Fan, W.M., 2008. Origin of clinopyroxene megacrysts in the late Mesozoic and Cenozoic basalts from the North China Craton and their constraints on the magma process of host rocks: a case of the Junan and Hebi. Acta Petrologica Sinica 24, 65–76 (in Chinese with English abstract).
Xu, Y.G., Lin, C.Y., Shi, L.B., Mercier, J.C.C., Ross, J.V., 1995. Upper mantle geotherm for eastern China and its geological implications. Science in China (B) 28, 525–542 (in Chinese).
Xu, P.F., Liu, F.T., Wang, Q.C., Cong, B.L., Chen, H., 2001. Slab-like high velocity anomaly in the uppermost mantle beneath the Dabie–Sulu orogen. Geophysical Research Letters 28, 1847–1850.
Xu, J.F., Castillo, P.R., Li, X.H., Yu, X.Y., Zhang, B.R., Han, Y.W., 2002a. MORB-type rocks from the Paleo-Tethyan Mian–Lueyang northern ophiolite in the Qinling Mountains, central China: implications for the source of the low $^{206}Pb/^{204}Pb$ and high $^{143}Nd/^{144}Nd$ mantle component in the Indian Ocean. Earth and Planetary Science Letters 198, 323–337.
Xu, P.F., Liu, F.T., Ye, K., Wang, Q.C., Cong, B.L., Chen, H., 2002b. Flake tectonics in the Sulu orogen in eastern China as revealed by seismic tomography. Geophysical Research Letters 29. doi:10.1029/2001GL014185.
Yaxley, G.M., Crawford, A.J., Green, D.H., 1991. Evidence for carbonatite metasomatism in spinel peridotite xenoliths from western Victoria, Australia. Earth and Planetary Science Letters 107, 305–317.
Yaxley, G.M., Green, D.H., Kamenetsky, V., 1998. Carbonatite metasomatism in the southeastern Australia lithosphere. Journal of Petrology 39, 1917–1930.
Ye, K., Cong, B.L., Ye, D.N., 2000. The possible subduction of continental material to depth greater than 200 km. Nature 407, 734–736.
Ying, J.F., Zhou, X.H., Zhang, H.F., 2004. Geochemical and isotopic investigation of the Laiwu–Zibo carbonatites from western Shandong Province, China, and implications for their petrogenesis and enriched mantle source. Lithos 75, 413–426.
Yu, X.H., Mo, X.X., Liao, Z.L., Zhao, X., Su, Q., 2001. Temperature and pressure condition of garnet lherzolite and websterite from west Qinling, China. Science in China (D) S 155–161.
Yu, X.H., Mo, X.X., Su, S.G., Dong, F.L., Zhao, X., Wang, C., 2003. Discovery and significance of Cenozoic volcanic carbonatite in Lixian, Gansu Province. Acta Petrologica Sinica 19, 105–112 (in Chinese with English abstract).
Yu, X.H., Zhao, Z.D., Mo, X.X., Wang, Y.L., Xiao, Z., Zhu, D.Q., 2004. Trace element, REE and Sr, Nd, Pb isotopic geochemistry of Cenozoic kamafugites and carbonatite from west Qinling, Gansu Province: implication of plume–lithosphere interaction. Acta Petrology Sinica 20, 483–494 in Chinese with English abstract.
Yu, X.H., Zhao, Z.D., Mo, X.X., Zhou, S., Zhu, D.Q., Wang, Y.L., 2005. $^{40}Ar/^{39}Ar$ dating for Cenozoic kamafugites from western Qinling in Gansu Province. Chinese Science Bulletin 50, 2638–2643.
Zangana, N.A., Downws, H., Thirlwall, M.F., Marker, G.F., Bea, F., 1999. Geochemical variation in peridotite xenoliths and their constituent clinopyroxenes from Ray Pit (French Massif Central): implications for the composition of the shallow lithospheric mantle. Chemical Geology 153, 11–35.
Zhang, H.F., 2005. Transformation of lithospheric mantle through peridotite–melt reaction: a case of Sino–Korean craton. Earth and Planetary Science Letters 237, 768–780.
Zhang, H.F., 2006. Peridotite–melt interaction: an important mechanism for the compositional transformation of lithospheric mantle. Earth Science Frontiers 13, 65–75 (in Chinese with English abstract).
Zhang, Q., Zhou, G.Q., 2001. Ophiolites of China. Science Press, pp. 16–68 (in Chinese).
Zhang, G.W., Zhang, B.R., Yuan, X.C., Xiao, Q., 2001. Qinling Orogenic Belt and Continental Dynamics. Science Press, pp. 1–855 (in Chinese).
Zhang, G.W., Dong, Y.P., Yao, A.P., 2002a. Some thoughts on study of continental dynamics and orogenic belt. Geology in China 29, 7–13 (in Chinese with English abstract).
Zhang, Z.C., Xiao, X.C., Wang, J., Wang, Y., 2002b. Discovery of enclaves from Cenozoic Pulu volcanic rocks of west Kunlun Mountains and their geological implications. Earth Science-Journal of China University of Geosciences 27, 386–390 (in Chinese with English abstract).
Zhang, H.F., Sun, M., Zhou, M.F., Fan, W.M., Zhou, X.H., Zhai, M.G., 2004. Highly heterogeneous Late Mesozoic lithospheric mantle beneath the North China Craton: evidence from Sr–Nd–Pb isotopic systematics of mafic igneous rocks. Geological Magazine 141, 55–62.
Zhang, H.F., Nakamura, E., Kobayashi, K., Zhang, J., Ying, J.F., Tang, Y.J., Niu, L.F., 2007a. Transformation of subcontinental lithospheric mantle through peridotite–melt reaction: evidence from a highly fertile mantle xenolith from the North China craton. International Geology Review 49, 658–679.
Zhang, X.M., Sun, R.M., Teng, J.W., 2007b. Study on crustal, lithospheric and asthenospheric thickness beneath the Qinghai–Tibet Plateau and its adjacent areas. Chinese Science Bulletin 52, 797–804.
Zhang, H.F., Goldstein, S.L., Zhou, X.H., Sun, M., Zheng, J.P., Cai, Y., 2008. Evolution of subcontinental lithospheric mantle beneath eastern China: Re–Os isotopic evidence from mantle xenoliths in Paleozoic kimberlites and Mesozoic basalts. Contributions to Mineralogy and Petrology 155, 271–293.
Zheng, J.P., Zhang, R.Y., Griffin, W.L., O'Reilly, S.Y., 2005. Heterogeneous and metasomatized mantle recorded by trace elements in minerals of the Donghai garnet peridotites, Sulu UHP terrane, China. Chemical Geology 221, 243–259.
Zhou, M.D., Lu, T.Y., Zhang, Y.S., Ruan, A.G., 2000. The geological structure background and the crustal structure in the northeastern margin of the Qinghai–Tibetan plateau. Acta Seismologica Sinica 22, 645–653 (in Chinese with English abstract).
Zindler, A., Hart, S.R., 1986. Chemical geodynamics. Annual Review of Earth and Planetary Sciences 14, 493–571.